EXPERIMENTAL INVESTIGATION OF N_2O/O_2 MIXTURES AS VOLUMETRICALLY

EFFICIENT OXIDIZERS FOR SMALL SPACECRAFT HYBRID PROPULSION

SYSTEMS

by

Rob L. Stoddard

A thesis submitted in partial fulfillment
of the requirements for the degree

of

MASTER OF SCIENCE

in

Mechanical Engineering

Approved:

_____   _____
Stephen A. Whitmore, Ph.D.   David Geller, Ph.D.
Major Professor   Committee Member

_____   _____
Geordie Richards, Ph.D.   Richard S. Inouye, Ph.D.
Committee Member   Vice Provost for Graduate Studies

UTAH STATE UNIVERSITY
Logan, Utah

2019

ABSTRACT

Experimental Investigation of N_2O/O_2 Mixtures as Volumetrically Efficient Oxidizers for

Small Spacecraft Hybrid Propulsion Systems

by

Rob L. Stoddard, Master of Science

Utah State University, 2019

Major Professor: Stephen A. Whitmore, Ph.D.
Department: Mechanical and Aerospace Engineering

Hydrazine has been a widely used primary propellant for small spacecraft systems. However, hydrazine is toxic and explosive, requiring special procedures to ensure safety during handling. With the special care required, hydrazine has quickly become unaffordable for the emerging, non-defense spacecraft industry. NASA and the Department of Defense have actively solicited research projects to develop safer "green" propellant options to replace hydrazine. Answering these solicitations, the Propulsion Research Laboratory at Utah State University has developed a hybrid rocket system that is a feasible "green" alternative to hydrazine.

The Utah State University hybrid rocket system uses 3D printed acrylonitrile butadiene styrene as the fuel. When this fuel is 3D printed and a high-voltage, low-wattage current is applied to the material, an electrostatic arc is produced along the surface. This arc causes a small amount of fuel to pyrolyze. When an oxidizer, most-commonly gaseous oxygen, is introduced to the pyrolyzed fuel, joule-heating initiates combustion and results in immediate full-motor ignition.

This technology can serve as a low-cost replacement for hydrazine. However, because oxygen possesses low-density, it must be stored at high-pressure levels to be volumetrically

efficient. The high-pressure levels introduce a fire and explosion hazard requiring special cleaning of spacecraft components, and aerospace components rated for gaseous oxygen must be used. These requirements are dis-advantageous for operational systems. One alternative is to use nitrous oxide in place of oxygen as the oxidizer in the system.

At normal temperatures nitrous oxide is a two-phase solution existing as a liquid and gas. Nitrous oxide in liquid form is inert, but in vapor form at high temperatures, can experience a rapid and energetic decomposition reaction. In pure form, nitrous oxide vapor has a high thermal decomposition energy barrier, but if contaminated by hydrocarbon residue, this barrier is reduced, allowing decomposition to occur at low temperatures. Dissolving oxygen into nitrous oxide dilutes the vapor ullage and reduces the decomposition hazard. The product, "Nytrox", provides a high-density, low-pressure option that is safely stored at room temperature.

This thesis will investigate the viability of replacing oxygen with nitrous oxide/oxygen mixtures. Research objectives and goals are presented along with accomplishments.

(82 pages)

PUBLIC ABSTRACT

Experimental Investigation of N_2O/O_2 Mixtures as Volumetrically Efficient Oxidizers for

Small Spacecraft Hybrid Propulsion Systems

Rob L. Stoddard

A hybrid thruster system utilizes propellants in two different stages, traditionally a solid fuel and a gaseous or liquid oxidizer. Recently hybrid thrusters have become a popular topic of research due to the high demand of a "green" replacement for hydrazine. Not only are hybrid thruster systems typically much safer than hydrazine, but they are also a low-cost system with a high reliability in performance. The Propulsion Research Laboratory (PRL) at Utah State University (USU) has developed a hybrid thruster system using 3-D printed acrylonitrile butadiene styrene (ABS) as the fuel and gaseous oxygen (GOX) as the oxidizer. This system has been spaceflight flown and tested in a hard vacuum environment with success. However, GOX has a low density and must be stored at high pressures to be considered viable. This thesis investigates the use of N_2O/O_2 mixtures, "Nytrox", and more commonly known as "laughing gas", as a higher density replacement oxidizer for GOX. In a manner directly analogous to the creation of soda-water using dissolved carbon dioxide, Nytrox is created by bubbling gaseous oxygen under high pressure into nitrous oxide until the solution reaches saturation level. Oxygen in the mixture ullage dilutes the nitrous oxide vapor, and increases the required decomposition activation energy of the fluid by several orders of magnitude. Data from tests using each oxidizer are analyzed and presented for performance comparisons. Comparisons include, ignition reliability, ignition energy, thrust coefficient, characteristic velocity, specific impulse, and regression rate. Nytrox is shown to work effectively as a "drop in" replacement for gaseous oxygen, exhibiting slightly reduced specific impulse and regression rate, but with the trade of a significantly higher volumetric efficiency.

ACKNOWLEDGMENTS

I want to thank Dr. Stephen Whitmore for all the help with the various projects that he entrusted to me throughout my employment. I want to thank him for seeing my potential as a senior and allowing me to work on the NASA University Student Instrumentation Project (USIP). I want to thank all my family and friends who have helped and inspired me throughout the years. Finally, I want to thank my wife, Cassie, for all of her sacrifice to help me succeed. Without her love and assistance throughout the years of school education none of this would have been possible.

Rob L. Stoddard

CONTENTS

LIST OF TABLES

LIST OF FIGURES

NOTATION

A_{burn}	Fuel Grain Surface Burn Area
A_c	Fuel Port Cross Sectional Area
A_{exit}	Nozzle Exit Area
A_{wall}	Wall Area in the Fuel Grain
A_1	Venturi Inlet Area
A_2	Venturi Throat Area
A^*	Cross Sectional Area at Which Local Flow Chokes
$\frac{A_{exit}}{A^*}$	Nozzle Expansion Ratio
C_d	Flow Discharge Coefficient
C_F	Thrust Coefficient
C_f	Skin Friction Coefficient
$C_{f_{blowing}}$	Skin Friction Coefficient for Blowing Flow
C_{f_0}	Skin Friction Coefficient for Normal Boundary Layer Flow
C_p	Specific Heat at Constant Pressure
C_v	Specific Heat at Constant Volume
c_{exit}	Effective Exhaust Velocity
c^*	Characteristic Velocity of Propellants
F	Thrust
$\bar{G}_{ox}$	Oxidizer Massflux
$\bar{G}_{tot}$	Total Massflux
g_0	Nominal Acceleration of Gravity at Sea-Level
h_v	Latent Heat of Vaporization
$h_{v_{fuel}}$	Latent Heat of Vaporization of the Fuel Grain
h_f	Heat of Formation

$\Delta h_{surface}$	Temperature Difference Between the Flame and Fuel Grain Surface
I_{sp}	Specific Impulse
L_{fuel}	Fuel Grain Length
L_{port}	Fuel Grain Port Length
$\mathfrak{M}_f$	Mole or Volume Fraction of one Species in a Binary Gas Mixture
M_{exit}	Exit Plane Mach Number
M_w	Molecular Weight
ΔM_{fuel}	Consumed Fuel Mass
$\dot{m}_{fuel}$	Fuel Massflow
$\dot{m}_{ox}$	Oxidizer Massflow
$\dot{m}_{propellant}$	Propellant Massflow
$\dot{m}_{total}$	Total Massflow Through The Nozzle
O/F	Oxidizer-to-Fuel Ratio
O/F_{actual}	Actual Oxidizer-to-Fuel Ratio
O/F_{stoich}	Stoichiometric Oxidizer-to-Fuel Ratio
P_{exit}	Exit Plane Static Pressure
P_r	Prandtl Number
P_0	Chamber Pressure
P_1	Venturi Inlet Pressure
P_2	Venturi Throat Pressure
P_∞	Ambient Pressure
$\dot{q}_{convection}$	Heat Change Rate Due to Convection
Re_L	Reynolds Number
R_g	Gas Constant
R_u	Universal Gas Constant
r_L	Longitudinal Average of the Fuel Port Radius
r_0	Initial Fuel Port Radius

$\dot{r}_L$	Longitudinal Mean of the Fuel Regression Rate
$\bar{\dot{r}}$	Mean Regression Rate Over the Duration of the Burn
s_g	Specific Gravity
S_t	Stanton Number
T	Venturi Flow Path Temperature
T_{flame}	Flame Temperature
$T_{surface}$	Fuel Grain Port Surface Temperature
T_0	Stagnation Temperature
$T_{0_{actual}}$	Actual Stagnation Temperature
$T_{0_{ideal}}$	Ideal Stagnation Temperature
t_{burn}	Burn Time
t	Generic Time Symbol
U_e	Flow Velocity at Boundary Layer Edge
V_c	Fuel Grain Port Volume
β	Blowing Coefficient
γ	Ratio of Specific Heats
η^*	Combustion Efficiency
θ_{exit}	Conical Nozzle Exit Angle
μ_{ox}	Oxidizer Viscosity
ρ_{fuel}	Sold Fuel Density
ρ_{ox}	Oxidizer Density
$\rho \cdot I_{sp}$	Density Specific Impulse
τ_{wall}	Shearing Force on the Fuel Grain Wall
Φ	Equivalence Ratio

ACRONYMS

ABS	Acrylonitrile Butadiene Styrene
ADN	Ammonium Dinitramide
CEA	Chemical Equilibrium with Applications
DAQ	Data Acquisition
ECAPS	Ecological Advanced Propulsion Systems
EOS	Equation of State
ESTEC	European Space Agency Space Research and Technology Center
FDM	Fused Deposition Modeling
GOX	Gaseous Oxygen
HAN	Hydroxylamine Nitrate
HERO	Hazards of Electromagnetic Radiation Ordnance
HVPS	High Voltage Power Supply
IL	Ionic Liquids
LOX	Liquid Oxygen
MMH	Mono Methyl Hydrazine
NASA	National Aeronautics and Space Administration
NFPA	National Fire Prevention Agency
NI	National Instruments
NTO	Nitrogen Tetroxide
Nytrox XX	Nytrox Solution with XX% Nitrous Oxide In Liquid Phase
PPU	Power Processing Unit
PRL	Propulsion Research Laboratory
P&ID	Piping and Instrumentation Diagram
SSC	Swedish Space Corporation
TRL	Technology Readiness Level

UDMH   Unsymmetrical Di-Methyl Hydrazine

USAF   United States Air Force

USU   Utah State University

CHAPTER 1

INTRODUCTION

1.1 Background

The primary propellant used in most small-to-medium-sized satellites is hydrazine. Hydrazine is proven to be very reliable, but is also highly toxic, extremely explosive, and expensive. When a heat source is present or an oxidizer is introduced, the hydrazine may decompose spontaneously and detonate. When stored at standard temperature and pressure, hydrazine has a high vapor pressure causing complete vaporization. This vaporized hydrazine causes severe burns and permanent injury after contact with organic tissue. Due to the hazards that hydrazine presents, certain measures must be taken when handling and operating with hydrazine. The National Fire Prevention Agency [1] (NFPA) presents the hazards of hydrazine with their diamond classification.

Table 1.1: Hydrazine diamond classification from the NFPA [1]

Diamond	Hazard	Value	Description
	Health	4	Very short exposure could cause death or major residual injury.
	Flammability	4	Will rapidly or completely vaporize at normal atmospheric pressure and temperature, or is readily dispersed in air and will burn readily.
	Instability	3	Capable of detonation or explosive decomposition but requires a strong initiating source, must be heated under confinement before initiation, reacts explosively with water, or will detonate if severely shocked.
	Special		

With the current regulatory environment, the cost of commercial, non-defense use of hydrazine grows tremendously due to the hazards that are associated with its use. Cost

increases come from monitored controlled transport, storage, servicing, and cleanup when spills occur. When any toxic propellant is involved in a spacecraft, operations become extremely restricted and difficult. If a system modification is required close to the time of launch, then the work area must be evacuated while the hydrazine is removed. Handling of the removed hydrazine may only be done by trained workers in hazmat suites, these workers are the only ones allowed on-site during the process. With all the additional safety and procedures required, the cost of hydrazine increases [6]. The cost of hydrazine procurement is also growing, tybically exceeding \$100/lb [7]. Although this price is probably only for raw material and does not include transport, storage, or operation costs. Despite hydrazine being expensive, volatile, and environmentally unsustainable, defense-related companies continue to utilize it in satellite propulsion systems. This is because of the long shelf life and proven reliability in space applications.

Hydrazine has differing forms as a propellant that are used for varying applications depending on propulsion needs. For example, monomethyl hydrazine (MMH) and unsymmetrical dimethyl hydrazine (UDMH). Each form has slightly different performance metrics, such as: stable operating temperature range, heat of decomposition, and application use [8]. Hydrazine can be used in either a monopropellant or bipropellant system depending on performance or system complexity constraints. Monopropellant hydrazine has a vacuum specific impulse no higher than 225 s. Bipropellant hydrazine is used with either nitrogen tetroxide (NTO) or liquid oxygen (LOX) and has a maximum theoretical specific impulse of 303 s [8]. But the addition of NTO or LOX adds more operating costs and handling procedures for safe use. Therefore, the only propulsion system available to small satellites beyond hydrazine is a cold-gas system.

1.2 Recent Developments on "Green" Alternatives to Hydrazine

A study by the European Space Agency Space Research and Technology Center (ES-TEC) identified two essential design elements to acheiving low cost space access "1) Reduced production, operational, and transport costs due to lower propellant toxicity and explosion hazards, and 2) Reduced costs due to an overall reduction in subsystems complexity and

overall systems interface complexity. [9]" The study found the opportunity for operational cost savings by using simplified ground handling procedures. The study also highly recommended the development of a non-toxic, stable "green" alternative propellant.

In an attempt to answer the recommendation presented by ESTEC, the United States Air Force (USAF) and the Swedish Space Corporation (SSC) subsidiary Ecological Advanced Propulsion Systems (ECAPS) have been developing less toxic alternatives to hydrazine for the past decade. From this research two "green" propellants were highly developed and based on aqueous solutions of the ionic liquids (IL) Ammonium Dinitramide (ADN) [10] and Hydroxylamine Nitrate (HAN) [11].

At Edwards Air Force Base in California, USAF developed AF-M315E based on HAN [12]. AF-M315E has a long-duration system thermal management. This prevents freezing from occurring in the tanks, whereas hydrazine tanks must be heated at all times [13]. AF-M315E has been demonstrated to produce a vacuum I_{sp} of up to 245 seconds under steady state operating conditions, and is almost 50% more dense than monopropellant hydrazine [14]. Despite these advantages, AF-M315E systems must include tank and catalyst bed heaters. The tank heaters are used to heat the propellant before it enters the catalyst bed pre-heat system. In order to ensure reliable decomposition, the AFM-315E catalyst bed must be preheated to more than 400 °C, a process requiring 10-15 W of power for up to 10 minutes. Power levels for small satellites are limited thus making tank heaters an inefficient requirement.

AF-M315E does present a few notable safety advantages over hydrazine. Due to the higher viscosity of AF-M315E, chances of tank leakage are decreased and considered non-toxic when a leak does ensue. In the event of a leak, based on the Standard Practice for System Safety MIL-STD-882E [2], AF-M315E would only be considered "critical". Comparatively, a hydrazine leak, based on the same system, is considered "catastrophic". This is shown in Figure 1.2. Also, thrusters using AF-M315E cannot fire without the catalyst bed first being preheated.

In Sweden, ECAPS developed a second fuel which is based on ADN called LMP-103S.

Table 1.2: Standard Practice for System Safety MIL-STD-882E [2]

Severity Categories		
Description	Severity Category	Mishap Result Criteria
Catastrophic	1	Could result in one or more of the following: death, permanent total disability, irreversible significant environmental impact, or monetary loss equal to or exceeding $10M.
Critical	2	occupational illness that may result in hospitalization of at least three personnel, reversible significant environmental impact, or monetary loss equal to or exceeding $1M but less than $10M
Marginal	3	Could result in one or more of the following: injury or occupational illness resulting in one or more lost work day(s), reversible moderate environmental impact, or monetary loss equal to or exceeding $100K but less than $1M.
Negligible	4	Could result in one or more of the following: injury or occupational illness not resulting in a lost work day, minimal environmental impact, or monetary loss less than $100K.

Both of these fuels are safer and perform comparatively to hydrazine. While each fuel has its own advantages and disadvantages, NASA has shown interest in each. Through testing of each propellant, an analogy has been developed relating propellant systems to aircraft. No one aircraft is perfect for every need. Some aircraft are designed for speed, while others and built to transport cargo and passengers. When asked about which propellant would be used for future missions, NASA Marshall's Spacecraft Propulsion Systems Branch Chief, Charles Pierce, replied "NASA needs to have flexibility in the types of thrusters and propellant systems it has to meet a variety of mission needs. One type of propellant might work best for one type of mission while another is better suited for a different mission. It's important that we have choices as we go green" [15].

While both AF-M315E and LMP-103S are being called "green", the case can be made that they are far more toxic than a wide swath of other available options. A "green" propellant is considered "a high-performance, low-toxicity alternative to the state-of-the-art spacecraft propellant, hydrazine" [16]. AF-M315E is considered "critical" on the MIL-STD-882E scale, just one level under hydrazine at "catastrophic". The distinction between these two levels is relatively minimal. The category "catastrophic" means a spill could result in one or more of the following: death, permanent total disability, irreversible significant environmental impact, or monetary loss equal to or exceeding $10M. Whereas the category "critical" defines a spill as resulting in one or more of the following: permanent

partial disability, injuries or occupational illness that may result in hospitalization of at least three personnel, reversible significant environmental impact, or monetary loss equal to or exceeding \$1M but less than \$10M. A spill of AF-M315E is a long shot from being truly considered "green".

Hybrid thrusters show considerable ability to replace hydrazine as a "green" option. For decades, hybrid thrusters have been known for their safety and environmental friendliness [17]. Hybrid thrusters are of similar complexity to monopropellant systems since they require a single fluid flow path. However, a hybrid system, when properly optimized, have potential to provide the same performance level as a complex bi-propellant liquid system. Due to solid and liquid bi-propellant systems being developed more than seven decades, hybrid systems still remain at a low technology readiness level (TRL). As the need for a "green" replacement to hydrazine grows, the maturity of hybrid systems will grow resulting in a higher TRL.

1.3   USU High Performance Green Hybrid Propellant (HPGHP)

Since 2012, the Propulsion Research Lab (PRL) at USU has been researching a ABS/GOX hybrid thruster system. Through many research programs and a recent spaceflight onboard a sounding rocket, launched from NASA Wallops, this system has reached TRL 5. This hybrid thruster achieves an I_{sp} level that is 10% greater than NASA's pseudo-"green" alternatives. The PRL has tested multiple sizes of this thruster system with thrust levels ranging from 5 N to more than 900 N. The simplicity of this system allows for scalable fuel grains to be designed and fabricated.

Historically, hybrid thrusters use propellant that is relatively stable, this stability presents difficulty for ignition and restartability. Normally a pyrotechnic charge is used for motor ignition, but these charges are susceptible to the Hazards of Electromagnetic Radiation to Ordnance (HERO) [18]. Additionally, large pyrotechnic charges present an explosion hazard incompatible with many launch opportunities. Hybrid systems have the potential for restartability in flight, however if a pyrotechnic charge is used, this ability is unachievable since the charge is a "one-and-done" option.

(a) Scalable 3D Printed ABS
Fuel Grains

(b) Example Of Interlocking Fuel Grains
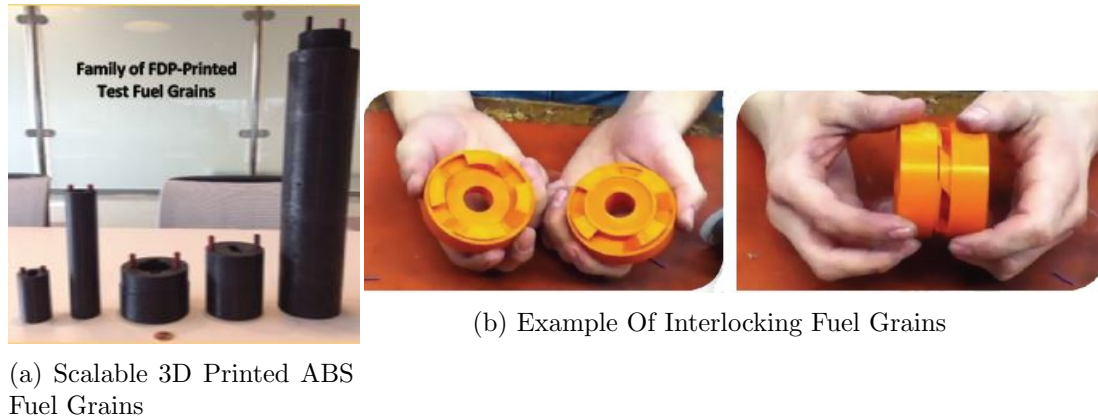
Fig. 1.1: Scalability and Versatility of 3D Printed ABS Fuel Grains

The issue of restartablility has been overcome by taking advantage of the unique electrical breakdown properties of different 3D printed thermoplastics. The PRL has discovered that Fused Deposition Modeling (FDM) processed ABS contains the unique electrical breakdown properties that can be used for fast on-demand ignition. ABS nominally holds a large high electrical resistivity and is not an electrical conductor. Although, as FDM-processed ABS is introduced to a electrostatic potential field the layered material structure concentrates minute electrical charges that result in arcing between the different layers of material. This arcing produces joule heating resulting in a highly conductive melt layer. After the melt layer is created, strong surface arcing is allowed for moderate voltage levels, between 200 and 300 volts. As the strong arcing continues, additional joule heating causes a small amount of material to vaporize. The vaporized fuel, when combined with oxidizing fuel, results in immediate motor combustion.

(a) Arc-Pyrolysis of Fuel

(b) Typical Motor Head-end Ignitor Layout

(c) Typical Arc-Ignition Systems Electronics Layout
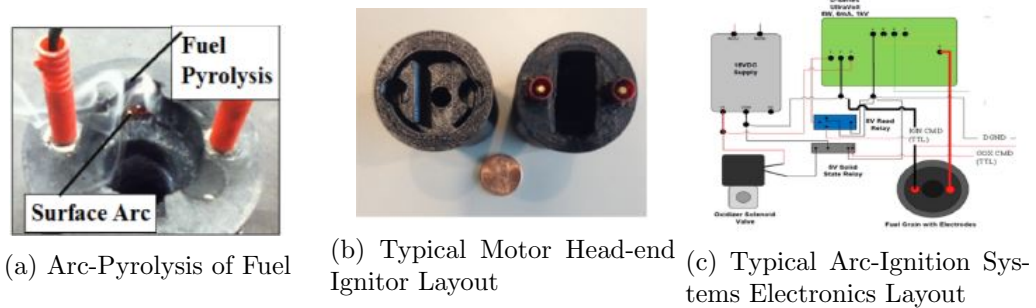
Fig. 1.2: 3D Printed Hybrid Arc-Ignition System Details [3]

Figure 1.2a presents a typical pyrolysis event, the vapor is the ablated hydrocarbon vapor from inductive arcing across the fuel material. The surface arc can also be seen. Figure 1.2b shows a typical motor head end layout with combustion shelf and electrodes installed. Figure 1.2c shows a baseline ignition system electronic setup.

Research at the PRL of this unique arc-ignition system has resulted in a power-efficient ignition system that has a high degree of reliability for restartability. This system developed entirely negates the hazards with electromagnetic radiation described in HERO. A pre-programmed process must take place making an inadvertent ignition of the motor nearly impossible.

1.4 Research Motivation

Figure 1.3 shows the numerous options of oxidizers for use in a hybrid thruster system, however only four options may be considered as "green": Liquid Oxygen (LOX), GOX, Hydrogen Peroxide (H_2O_2), and Nitrous Oxide (N_2O).
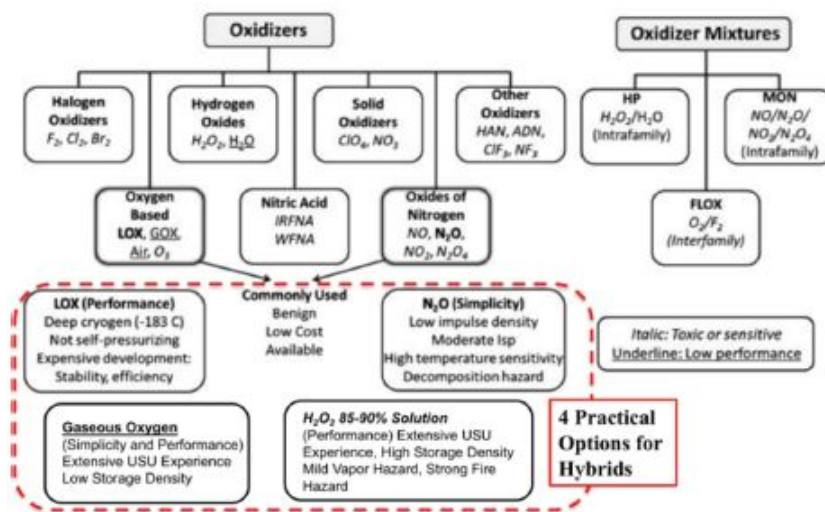
Fig. 1.3: Available Options for Hybrid Oxidizers [4]

To further compare these four oxidizers, calculations were made using NASA's Chemical Equilibrium Program (CEA) [19]. Comparisons were made concerning the characteristic velocity, c^*, flame temperature, specific gravity, and the product of the mean effective

propellant density ρ and c^*, called the density velocity, ρ^*. As can be seen in Figure 1.4, LOX is the best oxidizer when comparing performance metrics. When factoring in storage and safety measures for LOX it must be eliminated. The boiling point of LOX is $-297°F(-183°C)$, and therefore must be stored in a cryogenic tank with insulation from surrounding heat. LOX also requires special equipment for handling and storage [20].

(a) Characteristic Velocity vs. O/F Ratio

(b) Flame Temperature vs. O/F Ratio

(c) Specific Gravity vs. O/F Ratio

(d) Density Velocity vs. O/F Ratio
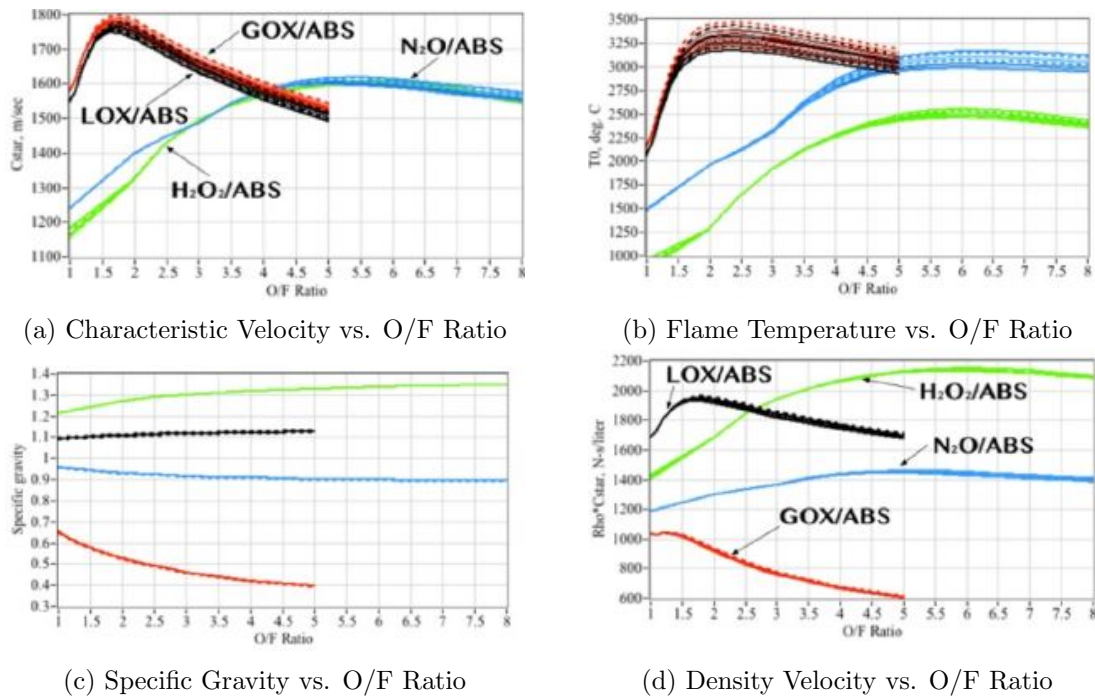
Fig. 1.4: Performance Comparison of Green Hybrid Oxidizers [3]

Significant research has been done by the PRL with high grade (90%) hydrogen peroxide. Unfortunately, hydrogen peroxide, while dense and very efficient, possesses many disadvantages making it impractical for in-space applications. Hydrogen peroxide is difficult to ignite unless used at high concentrations (>98%). Significant propellant pre-heat and conditioning must happen for successful ignition. Additionally, ignition time latencies occur before full combustion is achieved.

In the PRL, the main study of research has been focused on GOX as an oxidizer. GOX makes an excellent oxidizer and is extremely safe. The largest disadvantage to using GOX is the low levels of density. To overcome this issue, GOX must be stored at high pressure

levels. This prevents GOX from being a truly viable candidate to replace hydrazine for long-term space missions. Therefore, the only other option is nitrous oxide.

Nitrous oxide is the most commonly used oxidizer for hybrid thruster systems and is relatively inexpensive. The United States Occupational Safety and Health Administration (OSHA) has classified nitrous oxide as non-explosive, and non-flammable [21], and it is non-toxic to organic tissue. With these classifications, nitrous oxide is a clear front runner for a "green" replacement to hydrazine.

There are some hazards associated with nitrous oxide, such as the rapid decomposition of the vapor form. The hazards from working with nitrous oxide can be mitigated by using the gaseous solution of 50% by volume N_2O and 50% O_2. This mixture is used by the medical and dental community as an anesthesia. The introduction of O_2 results in the system being safer, larger ignition energy required for reaction, safe partial self-pressurization at high densities, and improved I_{sp} compared to pure N_2O. The hybrid solution of N_2O/O_2 has a slightly lower density than pure N_2O, but this results in a slight enhancement in I_{sp} levels and a reduction in the oxidizer-to-fuel ratio (O/F). N_2O/O_2 can safely be used with levels of O_2 as low as 10% and N_2O as high as 90% by volume.

CHAPTER 2

Nytrox Solution Model and Creation

2.1   Peng-Robinson Model

Mixtures of N_2O/O_2 can be purchased as a single-cylinder system under different brand names such as Entonox®. However, due to FDA regulations these systems are unavailable for purchase in the United States of America. Therefore, the medical community in the United States of America uses a system that combines the N_2O and O_2 from seperate tanks and delivers it to the patient as needed. This system, called Nitronox™, is expensive and does not provide the massflow levels required for USU's hybrid thruster. To overcome this the nytrox mixtures were made in-house.

(a) Vapor, Dissolved O_2 Fraction at Saturation   (b) Liquid, Dissolved O_2 Fraction at Saturation
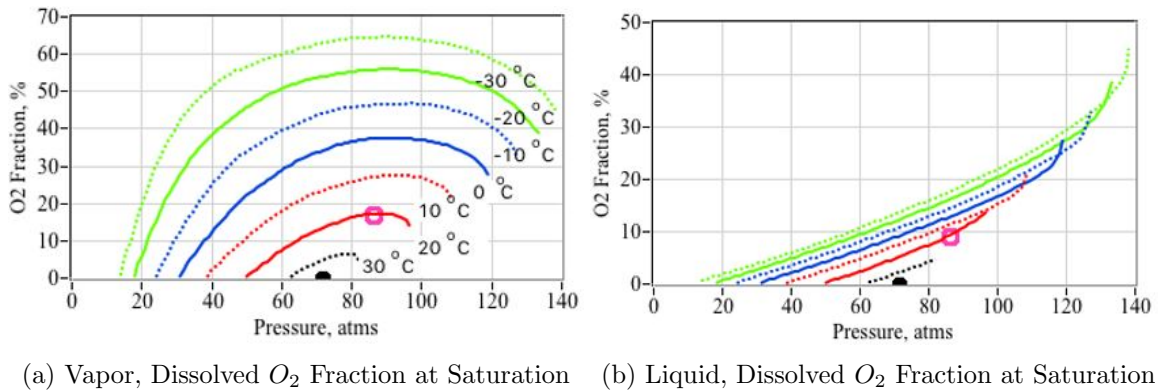
Fig. 2.1: Vapor and Liquid Mass Concentrations Of Oxygen In The Solution [3]

Figure 2.1 plots the vapor/liquid/isotherm diagram for a saturated N_2O/O_2 solution. These curves of Figure 2.1 were calculated using the Peng-Robinson model for two-phase binary solutions. The Peng–Robinson model is a higher-order equation of state that is widely used for two-phase systems, due to its accuracy at high pressure levels. This equation of state expresses fluid properties in terms of pressure, temperature and compressibility of each species involved. Due to the highly-polar nature of nitrous oxide, the model allows an

acentric factor to account for the the non-sphericity of the molecules. As the acentric factor increases increases, the vapor curve is "pulled" down, resulting in higher boiling points. At a given pressure and temperature, the equilibrium mixture composition results when the fugacities of each phase of for both nitrous oxide and oxygen are balanced. The fugacity of a real gas is equal to the pressure of an ideal gas which has the same temperature and molar Gibbs free energy as the real gas. Appendix A of this thesis details the computational sequence for nitrous oxide and GOX mixtures. This calculation reproduces the procedure laid out in ref. [4]. Eq. (A8) of Ref. [4] has a typographical error that was discovered and reported by the author. The corrected equation is used for the calculations of Figure 2.1.

Figure 2.1a plots the vapor and 2.1b plots the liquid phase mass concentrations of oxygen in the solution as a function of saturation pressure. Isotherm curves for temperatures varying from -30 °C to 30 °C are shown. The 0 °C isotherm is highlighted as the solid blue line for both the liquid and vapor segments of the chart. There exists a "sweet spot", at 0 °C and 86 atmospheres (1250 psig), where the concentration of gaseous oxygen in the ullage is a maximum, approximately 37%, while the oxygen fraction in the liquid phase remains relatively low, approximately 13%. This optimal point allows for the maximum proportion of vapor dilution while maintaining a high density for the liquid fluid. The O_2 provides two immediate safety benefits in the mixture.

First, the oxygen mixture in the ullage significantly dilutes the nitrous oxide vapor, and significantly diminishes any potential for a decomposition reaction. Figure 2.2 plots the minimum energy, E_i, required for a point source to start a self-sustaining deflagration wave in nitrous oxide with varying initial concentrations of oxygen. For pure nitrous oxide vapor this energy is only about 400-500 miliJoules; however, only a 10% O2 concentration increases E_i to a value greater than 5 joules, an order of magnitude increase. A 35% O_2 concentration – easily achievable at pressures above 100 atmospheres – increases E_i to greater than 1000 joules, increasing by a factor of more than 4000. Analytical studies performed by Karabeyoglu [4] have demonstrated that blended N_2O/O_2 vapor with at least 20% concentration of O_2 is virtually impossible to ignite using any conceivable ignition.
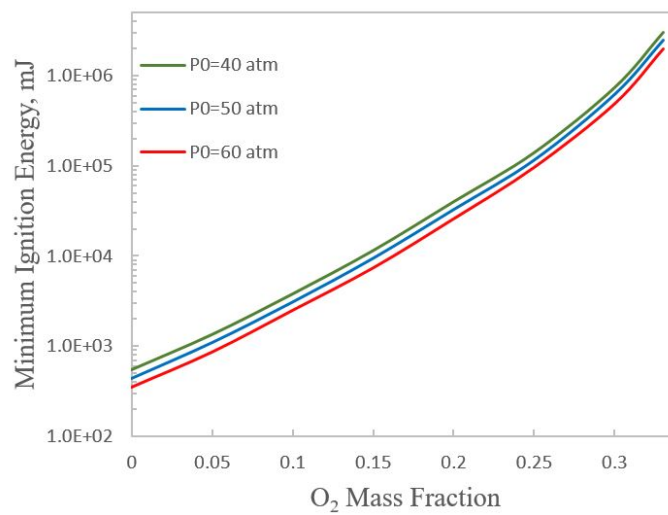
Fig. 2.2: Minimum Ignition Energy for N_2O/O_2 Mixtures at Three Pressure Levels [4]
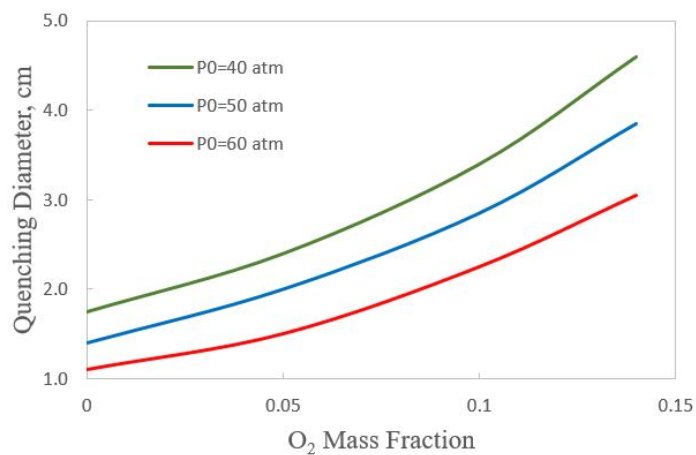

Fig. 2.3: Quenching Diameters for N_2O/O_2 Mixtures at Three Pressure Levels [4]

Second, the presence of O_2 in the solution significantly increases the "quench diameter," the diameter of a metal pipe that will quench any potential decomposition reaction and ensure that any potential deflagration wave will not propagate. Figure 2.3 shows this behavior. Note that the quench diameter for pure nitrous oxide is approximately 1.4 cm (0.6 in), and grows to more than 4.5 cm (1.77 in) for only 15% O_2 in solution. This difference is a factor of more than 8.7 in terms of the allowable piping cross sectional area. This allowable growth is quite significant in that it allows for substantially higher massflow levels in the system with no increase in deflagration risk.

(a) Vapor Density at Saturation Pressure   (b) Liquid Density at Saturation Pressure
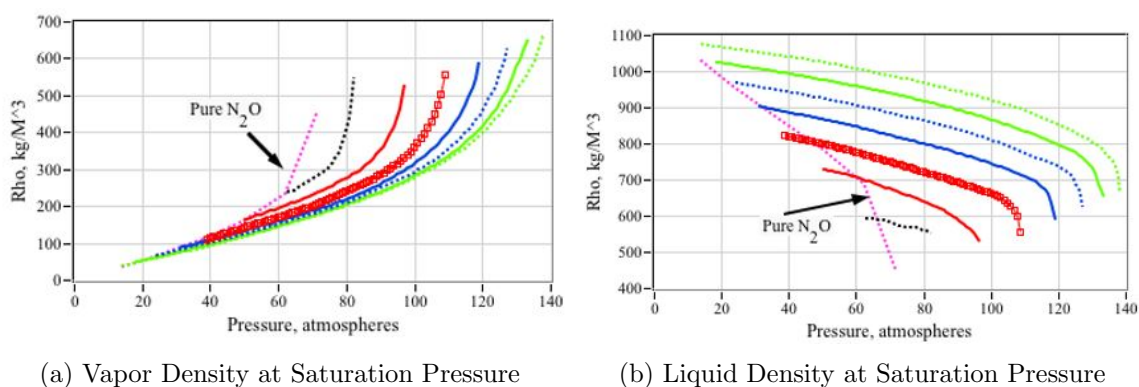
Fig. 2.4: Density of Nytrox Vapor and Liquid Phases vs. Vapor Pressure at Six Different Isotherms [3]

Figure 2.4 plots the densities of the vapor and liquid phases, as calculated by the Peng-Robinson model. Referring to Figure 2.1, at 0 °C a 90% mass concentration of N_2O in the liquid solution corresponds to a vapor pressure of approximately 75 atmospheres (1100 psia). At this vapor pressure the solution density is approximately 800 kg/m3. At a pressure of 120 atmospheres (1470 psia), the percentage of nitrous oxide in the liquid solution drops to only 70% with a corresponding density of only 590 kg/m3. This behavior seems counter-intuitive, but is the nature of two-phase binary solutions where the nitrous oxide and oxygen components become mutually dissolved in each other. This model was first developed in LabVIEW. The calculations of Figure 2.1 were performed using the Peng-Robinson [22] 2-phase state-equation for binary solutions. The implemented numerical algorithm follows

the procedure laid out by Karabeyoglu [4]. This method is further explained in Appendix A. The mixing rule used to combine the binary components is based on the model of Zudkevitch and Joffe [23]. For a fluid given temperature, the algorithm searches for the equilibrium pressure level that matches the fugacity of the vapor and liquid phases for each of the binary (O_2, N_2O) fluid components.

2.2   Nytrox Solution Processing Equipment and Fill Procedures

For this study highly-purified grades of nitrous oxide and gaseous oxygen were used in order to ensure the resulting Nytrox mixture was free from contaminants and any possible catalytic agents. The gas supplier quotes the N_2O purity at 99.7% by volume; with the primary impurities being traces of oxygen, nitrogen and water vapor. The GOX purity is quoted as 99.4 to 99.7%, with the main impurity being argon. Argon is not liquefiable at normal temperatures, and since argon's critical phase constants are so close to oxygen, its presence is considered negligible with regard to the mixing properties. Also, since argon is inert, there is no potential for catalytic effects.

The basic procedure consists of filling the run tank with the desired weight of N_2O, connecting the filled tank to a GOX supply, and allowing the GOX to bubble up through the liquid nitrous oxide. A dip tube is required on the run tank to allow GOX to percolate up through the liquid phase nitrous oxide without inverting the tank. The dip tube also allows direct delivery of liquid-phase Nytrox for the hot fire tests. During passage through the liquid N_2O, oxygen dissolves into solution and also droplets of nitrous oxide are carried up into the gas phase. The net result is that the volume of liquid in the cylinder steadily diminishes until equilibrium vapor and liquid phase proportions are reached for the fluid temperature.

The objective of the developed procedure was to generate a Nytrox solution that possesses a maximum concentration of oxygen in the vapor phase, while maintaining a high N_2O concentration in the liquid phase. This optimum occurs at approximately 86 atmospheres (1250 psig). The result is a "Nytrox 88" solution with a vapor phase O_2 concentration of 36%, and a liquid phase O_2 concentration of only 12%. For this equilibrium condition the

liquid-phase Nytrox 88 solution has a density of approximately 0.785 $\frac{g}{cm^3}$. This value is compared to a liquid-phase density of pure N_2O of 0.907 $\frac{g}{cm^3}$ at 0 °C, which is only 15% higher. Using the ideal gas law, GOX at the same temperature and pressure would have a density of only 0.120 $\frac{g}{cm^3}$, or more than 6.5 times less than dense than the Nytrox 88 solution.

Nytrox Fill Apparatus
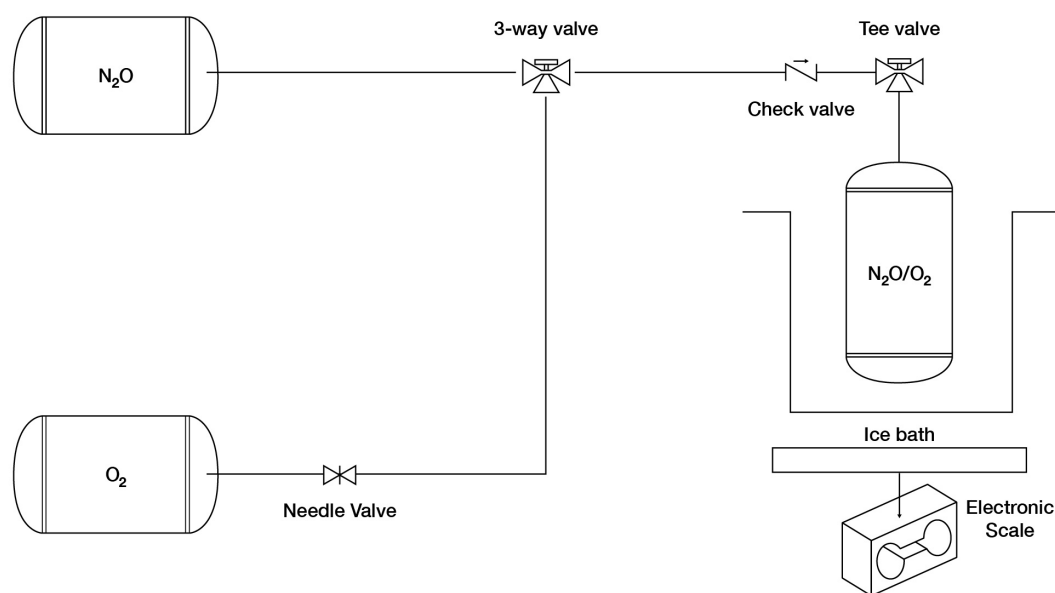
Fig. 2.5: Nytrox Percolation Apparatus Block Diagram [3]

The high grade N_2O is delivered in a K-size tank. The GOX-supply also comes delivered in a K-size tank with an internal pressure of 2000 psig. To ensure safety during the Nytrox mixing procedure, the pipes and fittings as procured were exclusively rated for Nitrous Oxide service. Also, all personnel present during the mixing process wore the proper safety equipment. The Nytrox was mixed in a commercial NOS® tank with a 10-lbm fill capacity, and designed for automotive applications. This particular unit comes with a pre-installed dip tube, has a design burst pressure of 8000 psig and a factory installed burst disc rated to 3000 psig. Safety of using this tank was verified since the pressures desired were well below

the burst disc pressure. All service lines were fabricated from braided stainless steel, and are specifically rated for nitrous oxide service.

N_2O Fill Procedure

Fig. 2.6: N_2O Fill Apparatus [3]

To begin the Nytrox manufacturing procedure, the NOS run tank is first filled with the desired amount of liquid nitrous oxide, typically 5-7 lbs. (1100-1,550 grams). To protect all personnel in the advent of an unlikely decomposition event, the N_2O fill procedure is performed in a wire cage. Figure 2.6 shows the NOS run tank fill apparatus. The NOS run tank was placed in an ice bath to lower the tank temperature to 0 °C, while the N2O K-service tank was kept at room temperature. The temperature difference created by the ice bath lowers the vapor of the fluid in the NOS run tank, creating a pressure difference that initiates in fluid flow. After ensuring that the needle valve and both tanks are closed.

The N_2O fill line is first securely fastened to both the service tank and the NOS run tank with the check valve allowing flow into the NOS run tank.

An electronic scale was used to measure the nitrous oxide mass moved from the service tank to the run tank. Before filling the empty tank, weight was recorded, and the scale was tared to give an initial reading of 0. The NOS run tank/ice bath combo is then placed on a scale used to measure the weight of N_2O added to the tank. With the needle valve closed, both the N_2O tank and the NOS run tank were opened. The needle valve was then opened slowly to allow flow of N_2O into the NOS run tank at a slow rate. Once the scale display reads the desired mass, the needle valve was closed, followed by the N_2O service tank and NOS run tank valves. Slowly disconnecting the fill line from each bottle allows lines to vent during removal.

Nytrox / O_2 Percolation Procedure

All gas mixing procedures were performed in the Battery Limits and Survivability Testing (Blast) Lab, USU's on campus jet engine and rocket test facility. This service bunker has 1-foot thick concrete walls with two 6" thick Plexiglas viewing pane from which test conductors can view hazardous operations directly in an indoors shirt-sleeve environment. Conveniently the Blast lab is located directly across the street from the PRL facility. Figure 2.5 shows the percolation apparatus block diagram, and Figure 2.7 shows the layout of the assembled system. Two different service lines are used for mixing the Nytrox. The fill line from the N_2O to the NOS run tank was approximately 8 ft. long consisting of the following components: four 2 ft. line sections, one N_2O filter to ensure cleanliness of N_2O, one backflow prevention (check) valve rated at 3000 psig, and one precision flow-adjustment (needle) valve rated at 2000 psig. The fill line from the O_2 to the NOS run tank was approximately 4 ft. long consisting of the following components: two 2 ft. line sections, one backflow prevention (check) valve rated at 3000 psig, a precision flow-adjustment (needle) valve rated at 2000 psig, and a pressure regulator rated at 3000 psig.

After ensuring that the needle valve and both tanks are closed, the O_2 fill line is attached to both the O_2 tank and the NOS run tank with the check valve allowing flow

Fig. 2.7: Assembled O_2 Percolation Apparatus [3]

into the NOS run tank. The O_2 tank is then opened and the pressure regulator is set to a downstream pressure of 1250 psig. The NOS run tank is then opened. Since a very slow flow of O_2 is desired into the NOS run tank, the needle valve is opened just until O_2 flow can be heard. This configuration is then left to allow the O_2 to percolate through the N_2O currently in the NOS run tank and reach a pressure equilibrium. Once pressure equilibrium is reached and the pressure in the NOS run tank is confirmed and the needle valve and both tanks are closed. As before, the service lines are slowly disconnected from each bottle allowing the line to vent during removal. Once the NOS run tank is filled, a final mass is logged before storing the Nytrox for future testing.

To further mitigate any potential risk of runaway decomposition reaction, the serviced NOS run tank is stored potable in a freezer unit to keep vapor pressures low and ensure a minimal amount of N_2O vapor in the tank ullage. By decreasing the temperature of the NOS run tank, the activation energy barrier is raised even further to prevent any accident

from occurring. Internal freezer temperatures are kept around –15° C. To ensure only trained personnel can handle the NOS run tank, a lock was installed on the freezer.

2.3   Nytrox Mixing Results

The procedures described were followed to generate the Nytrox batches used for this testing campaign. For each batch the NOS run tank was filled with 5 lb. (2.27 kg) of nitrous oxide, and allowed to chill in the ice bath. A 5 lb. fill is 1/2 of the rated fill capacity for NOS run tank. Once the tank temperature stabilized at 0 °C, the O_2 needle valve was opened and oxygen was allowed to percolate through the system. Once connected with the regulator set at 1250 psig, the process takes about 2 hours to reach equilibrium. Table 2.1 summarizes these processing results. The batch comparisons are remarkably similar as seen from the standard deviation[1] of each row. Thus, the established fill procedures were quite successful and worked as well as planned.

---

[1]The mean and standard deviation of each row was determined without consideration of Batch 6. Batch 6 is a slight outlier from the rest due to the O_2 tank have a low level of O_2 when the batch was made. There was not enough pressure to reach the target pressure of 1250 psig and the system reached equilibrium at 1163 psig. When excluding batch 6, the standard deviations fall lower.

Table 2.1: Nytrox Mix Batch Specifications

Nytrox Mix Batch Specifications								
Batch No.	1	2	3	4	5	6	Mean[1]	Std. Dev.[1]
NOS Tank Tare Weight (kg)	7.657	7.657	7.655	7.654	7.659	7.612	7.656	0.018
NOS Tank Internal Volume (L)	6.846	6.846	6.846	6.846	6.846	6.846	6.846	0.000
Final Tank Fill Pressure (kPa)	8704.4	8842.3	8739.4	8760.1	8725.6	8105.1	8754.36	269.294
Final Tank Fill Temperature (°C)	0	0	0	0	0	0	0.000	0.000
Final Filled Tank Weight (kg)	10.524	10.578	10.571	10.518	10.524	10.466	10.543	0.041
Oxidizer Added (kg)	2.867	2.921	2.916	2.864	2.865	2.854	2.887	0.029
Mean Oxidizer Density (g/cm^3)	0.419	0.427	0.426	0.418	0.418	0.417	0.422	0.004
N_2O Added to Tank (kg)	2.234	2.267	2.284	2.273	2.283	2.278	2.268	0.019
O_2 Added to Tank (kg)	0.633	0.654	0.632	0.591	0.582	0.576	0.618	0.032
Total O_2 Mass Fraction (%)	21.7	21.9	21.5	21.9	21.8	19.44	21.760	0.959
Liquid Density (L)	0.774	0.770	0.773	0.773	0.774	0.790	0.773	0.007
Vapor Density (L)	0.235	0.241	0.236	0.237	0.236	0.212	0.237	0.010
Liquid O_2 Mass Fraction (%)	12.63	12.99	12.72	12.78	12.69	11.13	12.762	0.678
Vapor O_2 Mass Fraction (%)	37.14	37.20	37.16	37.17	37.16	36.40	37.166	0.313
Liquid Mol. Weight (g/mol)	41.43	41.37	41.42	41.41	41.42	41.71	41.41	0.124
Vapor Mol. Weight (g/mol)	37.67	37.66	37.67	37.67	37.67	37.77	37.668	0.042
Mass of Liquid in Tank (kg)	1.807	1.851	1.869	1.789	1.799	1.915	1.823	0.049
Mass of Vapor in Tank (kg)	1.060	1.070	1.047	1.075	1.066	0.939	1.064	0.052
Volume of Liquid in Tank (L)	2.334	2.403	2.418	2.316	2.326	2.425	2.359	0.050
Ullage Volume in Tank (L)	4.512	4.443	4.429	4.530	4.520	4.421	4.487	0.050
Mix Quality in Tank (%)	0.370	0.366	0.359	0.375	0.372	0.329	0.368	0.017

CHAPTER 3

HYBRID ROCKET THEORY

3.1 Massflow Rates

3.1.1 GOX Massflow Computation

For the GOX mass flow sensor, the massflow calculation was rather straight forward, and the compressible venturi massflow equations are derived from material presented by Anderson [24] (Chapter 3, pp. 65-121). The stagnation pressure is calculated from the inlet P_1 and throat P_2 absolute pressure levels, and the venturi inlet A_1 and throat flow areas A_2.

$$P_0 = \left[\frac{\left(\frac{A_1}{A_2} \right)^2 (P_1)^{\frac{\gamma+1}{\gamma}} - (P_2)^{\frac{\gamma+1}{\gamma}}}{\left(\frac{A_1}{A_2} \right)^2 (P_1)^{\frac{2}{\gamma}} - (P_2)^{\frac{2}{\gamma}}} \right] \tag{3.1}$$

Once the true inlet stagnation pressure is calculated, then the achieved massflow is calculated using the un-choked compressible massflow equation

$$\dot{m}_{ox} = C_d \cdot A_1 \cdot \sqrt{ \left(\frac{2\gamma}{\gamma-1} \right) \frac{1}{R_g \cdot T} \left[\left(\frac{P_1}{P_0} \right)^{\frac{2}{\gamma}} - \left(\frac{P_1}{P_0} \right)^{\frac{\gamma+1}{\gamma}} \right] } \tag{3.2}$$

The calculation of Eq. 3.1 requires a temperature measurement T, this value is the temperature of oxidizer flowing into the venturi meter. The flow discharge coefficient C_d accounts for frictional flow losses.

3.1.2 Nytrox Massflow Computation

In contrast to the GOX flow, due to the two-phase, binary fluid nature of the Nytrox solution flow, deriving meaningful massflow measurements from the venturi sensor is rather more complicated. Multiple models have been previously developed for two phase nitrous

oxide mass flows. These include models developed by Zilliac and Karabeyoglu [25], Dyer [26], Whitmore and Chandler [27], Zimmerman, et.al [28], and Waxman et. al [29]. It is likely that these models, each developed for the flow of a single saturated liquid are applicable to the two phase binary fluid injector problem, but a solid theoretical foundation for this adaptation has yet to be developed. Thus, for this preliminary proof-of-concept testing campaign, the Nytrox massflow through the venturi was modeled as a simple compressible gas flow with a calibrated discharge coefficient. Here, an ideal gas is assumed with the gas properties derived from vapor phase mole fraction as calculated by the Peng-Robinson model (Ref. [4]). The associated ideal gas thermodynamic properties are

- Molecular Weight

$$M_{W_{Nytrox}} = \mathfrak{M}_{f_{N_2 0}} \cdot M_{w_{N_2 0}} + \mathfrak{M}_{f_{O_2}} \cdot M_{w_{O_2}} \tag{3.3}$$

- Gas Constant

$$R_{g_{Nytrox}} = \frac{R_u}{M_{w_{Nytrox}}} \tag{3.4}$$

- Specific Heat at Constant Pressure

$$C_{p_{Nytrox}} = \frac{\mathfrak{M}_{f_{N_2 0}} \cdot M_{w_{N_2 0}} \cdot C_{p_{N_2 O}} + \mathfrak{M}_{f_{O_2}} \cdot M_{w_{O_2}} \cdot C_{p_{O_2}}}{M_{w_{Nytrox}}} \tag{3.5}$$

- Ratio of Specific Heats

$$\gamma_{Nytrox} = \frac{C_{p_{Nytrox}}}{C_{v_{Nytrox}}} = \frac{C_{p_{Nytrox}}}{C_{p_{Nytrox}} - R_{g_{Nytrox}}} \tag{3.6}$$

In Eqs. 3.3 - 3.6 the symbol $\mathfrak{M}_f$ represents the mole fraction of a given vapor species and R_u represents the universal gas constant. Using these values for R_g and γ, the Nytrox massflow is calculated using Eqs. 3.1 and 3.2.

3.2   Regression Rate, O/F, and Equivalence Ratio

Although the inline venturi measures the oxidizer mass flow in real-time, the test stand that will be used can not measure real-time fuel mass flow. Thus, for the analysis to better match the data that will be gather for this testing campaign the "instantaneous" fuel mass flow rates were calculated as the difference between the measured nozzle exit and oxidizer mass flow rates,

$$\dot{m}_{fuel} = \dot{m}_{total} - \dot{m}_{ox} \tag{3.7}$$

It is assumed that the injector flow is choked. The nozzle exit mass flow was calculated from the measured chamber pressure P_0, nozzle throat area A^*, and the exhaust gas properties (flame temperature T_0, ratio of specific heat γ, molecular weight M_w, and specific gas constant R_g) using the 1-dimensional choking mass flow equation, (Anderson [20], Chapter 4).

$$\dot{m}_{total} = A^* \cdot P_0 \cdot \sqrt{\frac{\gamma}{R_g \cdot T_0} \cdot \left(\frac{2}{\gamma+1}\right)^{\frac{\gamma+1}{\gamma-1}}} \tag{3.8}$$

The mean longitudinal fuel regression rate was calculated from the fuel mass flow by,

$$\dot{r}_L = \frac{\dot{m}_{fuel}}{2\pi \cdot \rho_{fuel} \cdot r_L \cdot L} \tag{3.9}$$

Integrating Eq. 3.9 from the initial condition to the burn time solves for the instantaneous mean port radius,

$$r_L(t) = \sqrt{r_0^2 + \frac{1}{\pi \cdot \rho_{fuel} \cdot L} \int_0^t \dot{m}_{fuel} dt} \tag{3.10}$$

The terminal cross sectional area of the fuel port is,

$$A_c(t_{burn}) = \pi \cdot r_0^2 + \frac{\Delta M_{fuel}}{\rho_{fuel} \cdot L_{fuel}} \tag{3.11}$$

The mean fuel regression rate over the duration of the burn is calculated by

$$\bar{\dot{r}} = \frac{\Delta M_{fuel}}{\pi \cdot \rho_{fuel} \cdot L_{port} \cdot (r_{t_{burn}} + r_0) \cdot t_{burn}} \tag{3.12}$$

The mean oxidizer mass flux, total mass flux, O/F ratio, and equivalence ratio are estimated by

$$\bar{G}_{ox_{mean}} = \frac{\int_0^{t_{burn}} \dot{m}_{ox}(t) \cdot dt}{A_c \left(t_{burn}\right)} \tag{3.13}$$

$$\bar{G}_{ox_{total}} = \frac{\Delta M_{fuel}}{A_c \left(t_{burn}\right)} \tag{3.14}$$

$$\frac{O}{F} = \frac{\int_0^{t_{burn}} \dot{m}_{ox}(t) \cdot dt}{\Delta M_{fuel}} \tag{3.15}$$

$$\Phi = \frac{O/F_{stoich}}{O/F_{actual}} \tag{3.16}$$

For each time step in the burn time history, two-dimensional tables of thermodynamic and transport properties were interpolated to calculate the gas constant R_g, ratio of specific heats γ, and flame temperature T_0. The table of equilibrium properties of the GOX/ABS exhaust plume were developed by Whitmore et al. [30] with measured chamber pressure P_0, combustion efficiency η^*, and mean O/F ratio as independent look up variables for the tables. Reference [30] used NASA's industry standard chemical equilibrium code CEA code (Ref. [19]) to perform the calculations.

The corresponding oxidizer mass consumed during a prescribed burn was calculated by integrating the venturi mass flow time history over the burn duration. The mean O/F ratio over the burn duration was estimated by dividing the consumed oxidizer mass by the consumed fuel mass. By adjusting η^* the flame temperature was scaled

$$T_{0_{actual}} = \eta^{*2} \cdot T_{0_{ideal}} \tag{3.17}$$

To adjust nozzle-exit massflow and the resulting consumed fuel massflow,

$$\Delta M_{fuel} = \int_0^t \left(\dot{m}_{total} - \dot{m}_{ox} \right) dt \tag{3.18}$$

Adjusting input combustion efficiency upwards has the effect of increasing the calculated fuel mass consumption, and downwards decreases the calculated fuel mass consumption. The fuel massflow calculation starts with an assumed combustion efficiency of $\eta^* = 0.95$.

Once the total mass flow and combustion chamber properties were calculated as described above, the 1-dimensional de Laval flow equations (Anderson [24], Chapter 4) were used to calculate the exit plane Mach number, pressure, effective exhaust velocity, thrust, thrust coefficient, specific impulse, and characteristic velocity. The following flow sequence was used for the de Laval flow model

- Numerical Solution for Exit Plane Mach Number

$$\frac{A_{exit}}{A^*} = \frac{1}{M_{exit}} \left[\left(\frac{2}{\gamma+1} \right) \left(1 + \frac{\gamma-1}{2} M_{exit}^2 \right) \right]^{\frac{\gamma+1}{2(\gamma-1)}} \tag{3.19}$$

- Exit Plane Static Pressure

$$P_{exit} = \frac{P_0}{\left(1 + \frac{\gamma-1}{2} M_{exit}^2 \right)^{\frac{\gamma}{\gamma-1}}} \tag{3.20}$$

- Effective Exhaust Velocity

$$C_{exit} = \lambda_{exit} \cdot M_{exit} \cdot \sqrt{\frac{\gamma \cdot R_g \cdot T_0}{1 + \frac{\gamma-1}{2} M_{exit}^2}} + \frac{(P_{exit} - P_\infty) \cdot A_{exit}}{\dot{m}_{total}} \tag{3.21}$$

- Thrust and Thrust Coefficient

$$F = \dot{m}_{total} \cdot C_{exit} \tag{3.22}$$

$$C_F = \frac{F}{P_0 \cdot A^*} \tag{3.23}$$

- Specific Impulse, Characteristic Velocity, and Density Specific Impulse

$$I_{sp} = g_0 \cdot C_{exit} \tag{3.24}$$

$$c^* = \frac{P_0 \cdot A^*}{\dot{m}_{total}} \tag{3.25}$$

$$\rho \cdot I_{sp} = s_g \cdot g_0 \cdot I_{sp} \tag{3.26}$$

In Eq. 3.21 $\lambda_{exit} = \frac{1}{2}(1 + \cos\theta_{exit})$, where λ_{exit} is the momentum thrust correction factor and θ_{exit} is the conical nozzle exit angle. In Eq. 3.24 g_0 is the normal acceleration of gravity at sea level, $9.8067\frac{m}{s^2}$. For the $\rho \cdot I_{sp}$ calculation in Eq. 3.26, s_g is the mean effective specific gravity of the propellants, and is calculated as

$$s_g = \frac{s_{g_{ox}} \cdot O/F + s_{g_{fuel}}}{O/F + 1} \tag{3.27}$$

In Eq. 3.27 the parameter refers to the storage specific gravity of the oxidizer and not the downstream specific gravity.

3.3   CEA Model

Although the solution of O_2 into N_2O slightly reduces the density of the oxidizer, the overall effect includes moderate enhancement of the I_{sp} and a significant reduction of the optimal O/F ratio. This performance-trade makes the N_2O/O_2 solution only slightly less volumetrically efficient than when pure nitrous oxide is used. Figure 3.1 presents these performance comparisons. Plotted are the 3.1a characteristic velocity c*, 3.1b vacuum Isp, 3.1c specific gravity, and 3.1d density $\rho \cdot I_{sp}$, which is the product of the mean propellant effective density and the specific impulse. The plotted curves are for 5 different oxidizers when burned with 3-D printed ABS; GOX, pure N_2O, 90% N_2O/10% O_2, 70% N_2O/ 30% O_2, and 50% N_2O/ 50% O_2. For simplicity the Nytrox blends will be referred to by the mass-percentage of nitrous oxide in the fluid blend; respectively, Nytrox 90, Nytrox 70, and Nytrox 50.
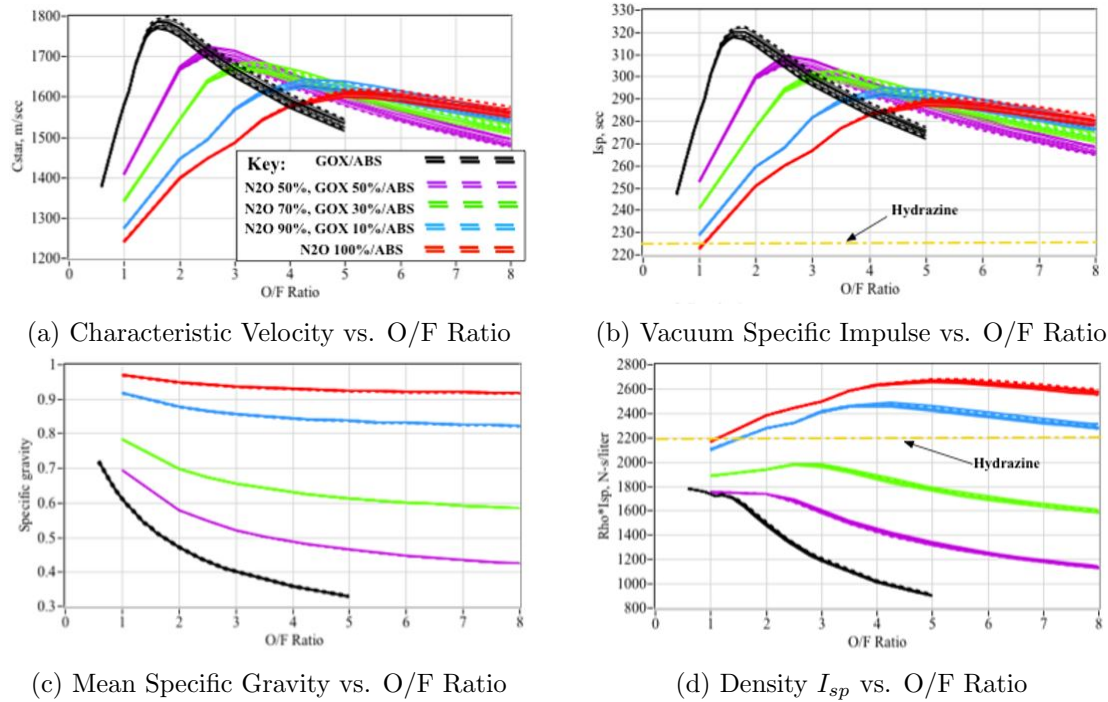
(a) Characteristic Velocity vs. O/F Ratio

(b) Vacuum Specific Impulse vs. O/F Ratio

(c) Mean Specific Gravity vs. O/F Ratio

(d) Density I_{sp} vs. O/F Ratio

Fig. 3.1: Performance of 3 Different N_2O/O_2 Concentrations Against Pure N_2O and GOX as Oxidizer [3].

The values plotted on Figure 3.1 were calculated using the CEA program, (Ref. [19]) assuming chamber pressures varying from 100 to 500 psia. The vacuum I_{sp} calculations assume a 40:1 nozzle expansion-ratio. The specific gravity calculation assumes a storage pressure of 1250 psig (86 atms), and fuel density of 1.04 $\frac{g}{cm^3}$. Also plotted on Figures 3.1b and 3.1d are the I_{sp} and $\rho \cdot I_{sp}$ of Hydrazine. Note that the hybrid mass I_{sp} performance significantly exceeds that of hydrazine. The density performance $\rho \cdot I_{sp}$ of the Nytrox 90 solution is greater than hydrazine, whereas the Nytrox 70 is slightly lower. As expected using GOX as the oxidizer results in the most mass-efficient system, but the low GOX storage density results in the lowest density impulse. Conversely using pure N_2O gives the best volumetric efficiency, but results in the lowest specific impulse and requires significantly more oxidizer in order to reach optimal Isp. The curve corresponding to the Nytrox 90 mixture (at 75 atmospheres vapor pressure) gives the best compromise with a distinct $\rho \cdot I_{sp}$ optimum occurring at an O/F ratio of approximately 4.2. As described previously, increasing the pressure to 84 atmospheres dilutes the nitrous oxide slightly more, but allows

the maximum percentage of dissolved oxygen in the vapor phase, and is an important consideration with regard to operational safety.

3.4 Nytrox/ABS Thruster Model

To predict the performance metrics of the hybrid thruster to be used a model was created in LabVIEW. The method used for the calculations in the model were similair yet slightly different from the methods described in Sections 3.1 and 3.2, which are data based calculations.

3.4.1 Ballistic Model

In state-space form the Nytrox/ABS ballistic thruster model includeds four equations; change in chamber pressure, change in chamber radius in the fuel grain, change in oxidizer used, and change in fuel used. The differential equation for the change of chamber pressure for the hybrid rocket model stems from the general rocket model equation

$$\frac{\partial P_0}{\partial t} + P_0 \left[\frac{1}{V_c} \frac{\partial V_c}{\partial t} + \frac{A^*}{V_c} \sqrt{\gamma R_g T \left(\frac{2}{\gamma + 1} \right)^{\frac{\gamma+1}{\gamma-1}}} \right] = \frac{R_g T_0}{V_c} [\dot{m}_{propellant}] \tag{3.28}$$

Where, for hybrid rocket motors, $\frac{\partial V_c}{\partial t} = A_{burn} \dot{r}_{fuel}$ and $\dot{m}_{propellant} = \dot{m}_{ox} + \rho_{fuel} A_{burn} \dot{r}_{fuel}$. A_{burn} is the grain surface burn area, $\dot{r}$ is the grain linear regression rate, and $\dot{m}_{ox}$ is the mass-flow rate of the oxidizer. It will be assumed that the flow is incompressible in the injector, therefore the massflow rate of the oxidizer can be represented by $\dot{m}_{ox} = A_2 C_d \sqrt{2\rho(P_1 - P_2)}$. Substituting these into Eq. 3.28 and rearranging results in the differential equation for the change in pressure with respect to time

$$\frac{\partial P_0}{\partial t} = \frac{A_{burn} \dot{r}_{fuel}}{V_c} [\rho_{fuel} R_g T_0 - P_0] - P_0 \left[\frac{A^*}{V_c} \sqrt{\gamma R_g T \left(\frac{2}{\gamma + 1} \right)^{\frac{\gamma+1}{\gamma-1}}} \right]$$
$$+ \frac{R_g T_0}{V_c} A_{ox} C_{d_{ox}} \sqrt{2\rho_{ox}(P_{ox} - P_0)} \tag{3.29}$$

In Eq. 3.29 the first term is the fuel vaporization term, the second term is due to choking massflow through the nozzle, and the third is the term explaining the oxidizer entering the combustion chamber. The only part that remains to be defined for Eq. 3.29 is $\dot{r}$. For solid rockets, this term is described by Saint Robert's Law, however this is inaccurate for hybrid rockets. Instead, the fuel regression rate in a hybrid rocket motor is proportional to the mass flux through the fuel grain port. The generic form is shown in Eq. 3.30.

$$\dot{r} = aG_{ox}^n \tag{3.30}$$

In Eq. 3.30 a and n are empirically derived constants that are dependent on the fuel material and oxidizer combination being used, G_{ox} represents the oxidizer mass flux. For an ideal hybrid rocket the value of n in Eq. 3.30 would be exactly 0.5. This would cause the O/F value to remain constant during the duration of the burn. However, with GOX/ABS and Nytrox/ABS mixtures thrusters $n \neq 0.5$ as will be shown later.

To better analyze the regression rate, the boundary layer inside the fuel grain must be interrogated. The boundary layer is shown in Fig. 3.2.
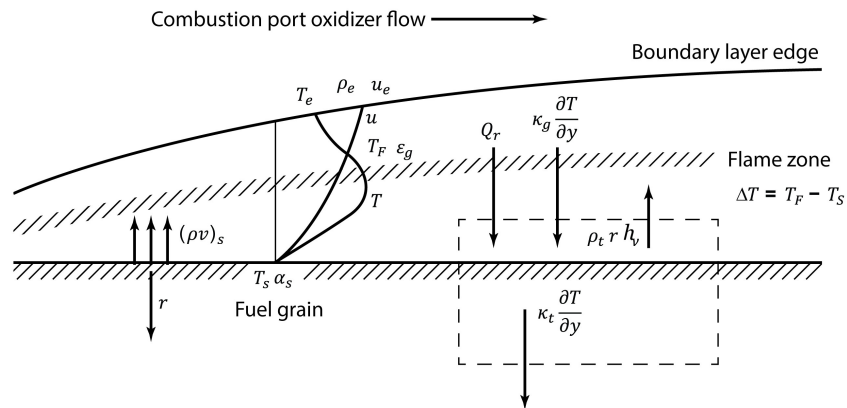

Fig. 3.2: Boundary Layer of Hybrid Rocket Fuel Grain [5]

The dotted line represents a control volume to be analyzed. The term $\frac{\partial T}{\partial y}$ ignores heat conduction and radiation into the solid fuel grain. From the control volume it can be seen that $\dot{q}_{convection} = \rho_{fuel}\dot{r}h_v = H\left[T_{flame} - T_{surface}\right] = S_t\rho_eU_e\Delta h_{surface}$. Where S_t is the Stanton number. Using Reynold's Analogy, which is a correlation of heat transfer to skin friction, the Stanton number can be expanded to be $S_t = \frac{C_f}{2}P_r^{-\frac{2}{3}}$, where C_f represents the skin friction coefficient. Solving for the regression rate results in Eq. 3.31

$$\dot{r} = \left(\frac{C_f}{2}P_r^{-\frac{2}{3}}\right)\left(\frac{\rho_eU_e}{\rho_{fuel}}\right)\left(\frac{\Delta h_{flame}}{h_f}\right) \tag{3.31}$$

During combustion, radial out gassing occurs from the fuel pyrolysis. This out gassing causes the flame zone to be pushed away from the fuel surface. To account for this a new coefficient β, blowing coefficient, needs to be introduced. The blowing coefficient is analogous to the wall shearing force due to radial outflow over the wall shearing force due to skin friction.

$$\beta = \frac{\dot{m}_{fuel}U_e}{\tau_{wall}A_{wall}} \tag{3.32}$$

Knowing that $\dot{m}_{fuel} = \rho_{fuel}A_{wall}\dot{r}$ and the denominator of Eq. 3.32 can be represented by $\tau_{wall}A_{wall} = \left(\frac{1}{2}\rho_eU_e^2\right)C_fA_{wall}$. Eq. 3.32 can be rearranged and simplified to the following

$$\beta = \left(\frac{\rho_{fuel}\dot{r}}{\rho_eU_e}\right)\frac{1}{C_f/2} \tag{3.33}$$

By using Reynold's Analogy again it is seen that $C_f/2 = S_tP_r^{\frac{2}{3}}$, therefore the final equation for the Blowing coefficient can be seen as

$$\beta = \frac{h_v}{\Delta h_{flame}}\frac{1}{P_r^{\frac{2}{3}}} \tag{3.34}$$

Using Lee's Empirical Correlation described in Appendix 4 of Sutton and Biblarz [5] it is shown that

$$\frac{C_{f_{blowing}}}{C_{f_0}} = 1.27 \left(\frac{h_v}{\Delta h_{flame}}\right)^{-0.77} \tag{3.35}$$

Plugging Eq. 3.35 into Eq. 3.31 results in

$$\dot{r} = \left(\frac{0.635}{P_r^{\frac{2}{3}}}\right) \left(\frac{\rho_e U_e}{\rho_{fuel}}\right) \left(\frac{\Delta h_{flame}}{h_f}\right)^{0.23} C_{f_0} \tag{3.36}$$

Where C_{f_0} represents the skin friction for normal boundary layer flow. From many years of testing hybrid rockets in the PRL, it has been noted that the inner wall of a fuel grain, post burn, very closely resembles that of a flat plate skin friction model. Therefore $C_f = \frac{0.075}{[R_{e_L}]}^{\frac{1}{5}}$ can be used. This results in the final version of $\dot{r}$ which is the second state equation needed.

$$\frac{\partial r}{\partial t} = \frac{0.047}{P_r^{\frac{2}{3}}\rho_{fuel}} \left(\frac{c_p\,[T_0 - T_{fuel}]}{h_{v_{fuel}}}\right)^{0.23} \left[\frac{A_{ox}C_{d_{ox}}}{A_c}\sqrt{2\rho_{ox}\,(P_{ox} - P_0)}\right]^{\frac{4}{5}} \left(\frac{\mu_{ox}}{L}\right)^{\frac{1}{5}} \tag{3.37}$$

The form of Eq. 3.37 matches the generic form presented in Eq. 3.30. The first two terms represent the resulting heat transfer, and in the generic from are represented by a. The third term is the oxidizer mass velocity, and in the generic form are represented by G_{ox} with $n = 4/5$. And the last term in Eq. 3.37 is a length parameter from the Reynold's number.

The final two state equations required for the model are very straight forward and can be defined as

$$\frac{\partial M_{ox}}{\partial t} = A_{ox}C_{d_{ox}}\sqrt{2\rho_{ox}\,(P_{ox} - P_0)} \tag{3.38}$$

$$\frac{\partial M_{fuel}}{\partial t} = \rho_{fuel}A_{burn}\dot{r} \tag{3.39}$$

These four state equations (Eq. 3.29, 3.37, 3.38, and 3.39) were used in a Runge-Kutta method to iterate for a prescribed amount of burn time for the motor. The results of each

iteration were then used to calculate performance metrics of the thruster. The results from the model are presented in Table 3.1 and Figure 3.3.

Table 3.1: Final Results From Nytrox/ABS Model

Mass of Fuel Burned (kg)	0.0087
Mass of Oxidizer Burned (kg)	0.0433
Total Mass Burned (kg)	0.0520
Mean O/F Ratio	5.0035
Mean I_{sp} (s)	230.812
Final Diameter In The Fuel Grain (m)	0.0153

The model was run with values for M_w, γ, T_0, and Pr being determined each time step from a 2-dimensional table of data from CEA. For this model the following were the inputs and assumed values.

Table 3.2: Inputs For The Nytrox/ABS Model

Nozzle Properties	
A/A*	2.07
θ_{exit} (degrees)	3.29
D_{exit} (m)	0.00483
D_{throat} (m)	0.00345

Injector Properties	
# of Ports	1
C_d	0.65
Pressure (Pa)	2.41E+06
D (m)	0.0011906

Other Input Values	
$P_{ambient}$ (Pa)	85814
t_{burn} (s)	4
dt (s)	1.00E-05

Viscosity Properties	
C_s (K)	240
T_s (K)	300
μ (Pa*s)	1.4889E-05

Fuel Grain Properties	
Length (m)	0.0508
d (m)	0.00515
ρ (kg/m^3)	1040
h_v (J/kg)	3.10E+06
Temperature (K)	300

Oxidizer Properties	
ρ (kg/m^3)	770.5
γ	1.4

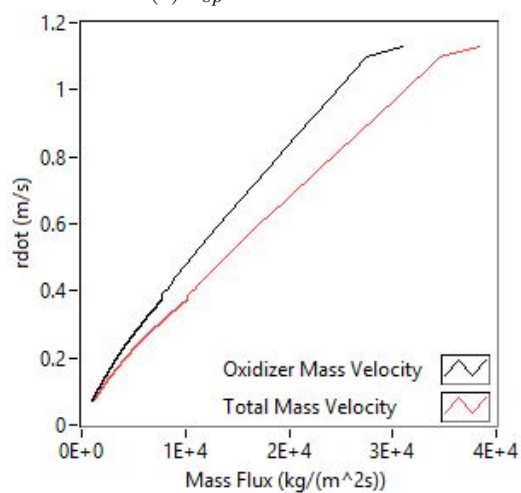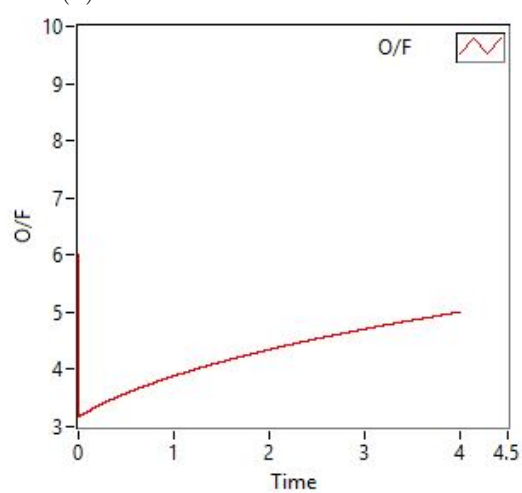| Assumptions Made	
Prandtl #	0.5
Combuster Efficiency	0.99
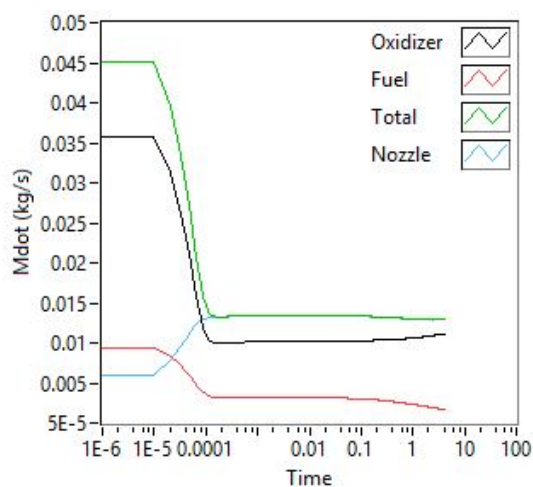
(a) $\dot{m}$ vs. Time
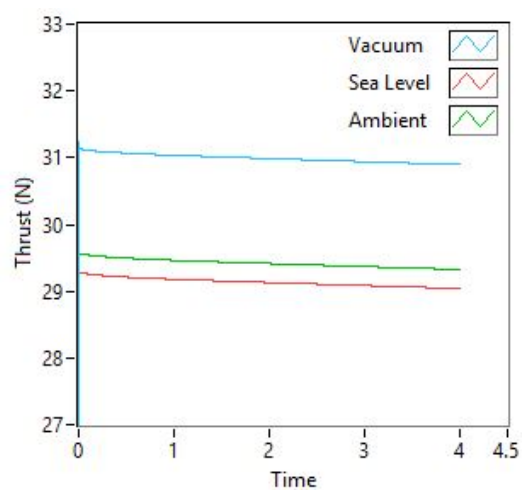
(b) Thrust vs. Time
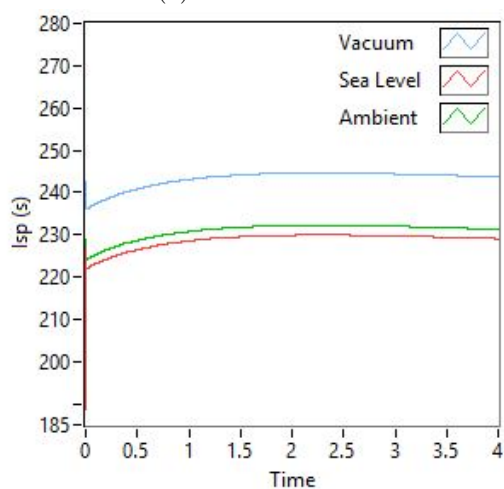
(c) I_{sp} vs. Time
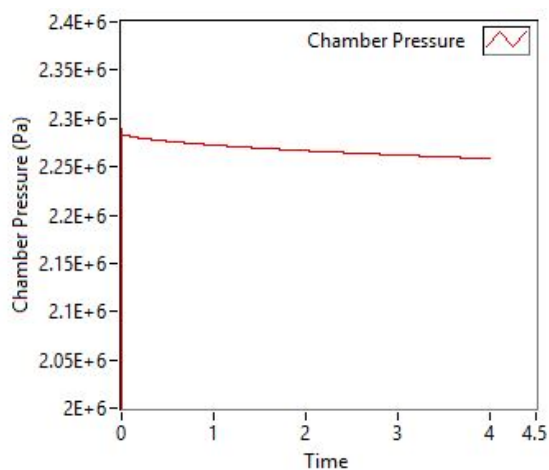
(d) Chamber Pressure vs. Time

(e) Linear Regression Rate vs. Mass Velocity

(f) O/F Ratio vs. Time

Fig. 3.3: Graphs Showing Results of Nytrox/ABS Model

CHAPTER 4

EXPERIMENTAL APPARATUS, INSTRUMENTATION, AND TEST APPARATUS

This chapter details the hardware, instrumentation and test procedures used to perform the hot fire evaluation tests. The hot fire testing campaign was performed using the previously-described Blast Lab test cell.

4.1 Thrust Chamber

The legacy GOX/ABS small spacecraft thruster of Refs. [31] and [32] was adapted for use in the testing campaign. Figure 4.1 presents the details of the thrust chamber assembly. Figure 4.1a presents a 2-D schematic. Figure 4.1b presents a photograph of the disassembled system. Depicted are the major components; i) graphite nozzle, ii) nozzle retention cap, iii) motor case, iv) 3D printed fuel grain with embedded electrodes, v) chamber pressure fitting, and vi) single-port injector cap. The 38-mm diameter thrust chamber is constructed from 6061-T6 high-temperature aluminum, and was procured commercially from Cesaroni Inc. Table 4.1 summarizes the thruster geometry and other specifications. The electronic arc-ignition system for this thruster was described previously and is depicted by Figure 1.2.
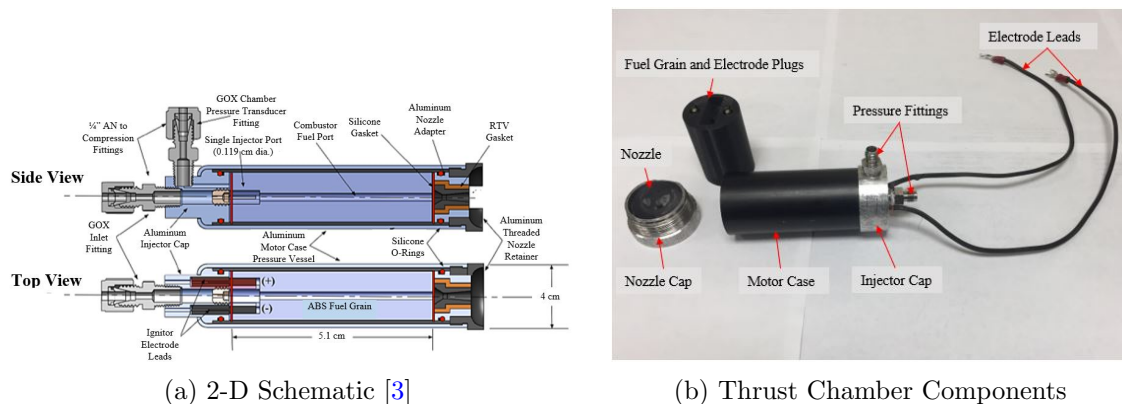

(a) 2-D Schematic [3]   (b) Thrust Chamber Components

Fig. 4.1: Test Article Thruster Assembly

Table 4.1: Motor Geometry and Parameter Specifications [3]

Parameter	Injector		Single Port, 0.119 cm (0.047 in.) Diameter	
Fuel Grain	Diameter: 3.168 (1.246 in.)	Length: 5.1 cm (2.0 in.)	Initial Weight: 45.0 g Print Density/Specific Gravity: 0.955	Initial Port Diameter: 0.53 cm (0.21 in.)
Motor Case	Diameter: 3.8 cm (1.50 in.)	Length: 7.92 cm (3.12 in.)	Wall Thickness: 1.5 mm (0.059 in.)	
Conical Graphite Nozzle	Initial Throat Diameter: 0.345 (0.014 in.)	Exit Diameter: 4.83 mm (0.17 in.)	Ambient Tests Initial Expansion Ratio: 2.07:1	Nozzle Exit Angle: 5.0 deg.

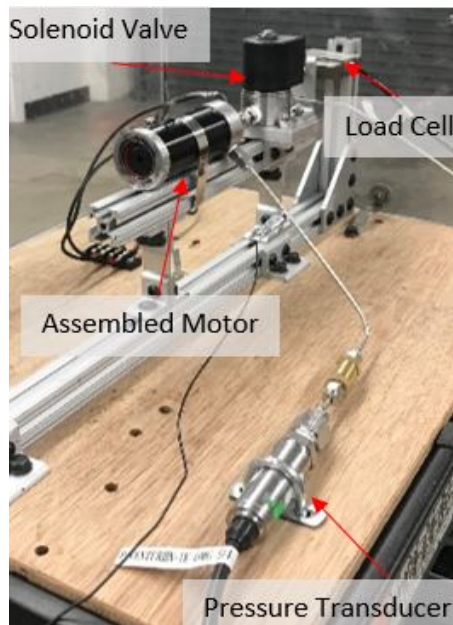## 4.2   Hot Fire Test Apparatus and Instrumentation

Fig. 4.2: Thruster Chamber Mounted to Load-Balance Test Sled

Figure 4.2 shows the flight weight motor assembled and mounted to the test load balance, ready for testing. Figure 4.3 shows the piping and instrumentation diagram (P&ID) of the test systems. Test stand measurements include venturi-based GOX massflow measurements, load-cell based thrust measurements, chamber pressure, and multiple temperature readings at various points along the flow path. The differential venturi pressure transducer

was installed to increase the accuracy of the sensed pressure drops. The thrust-stand support members allow bending along the direction of thrust to prevent them from interfering with the measured load. The entire test assembly is made using commercially available T-slot extruded-aluminum components.
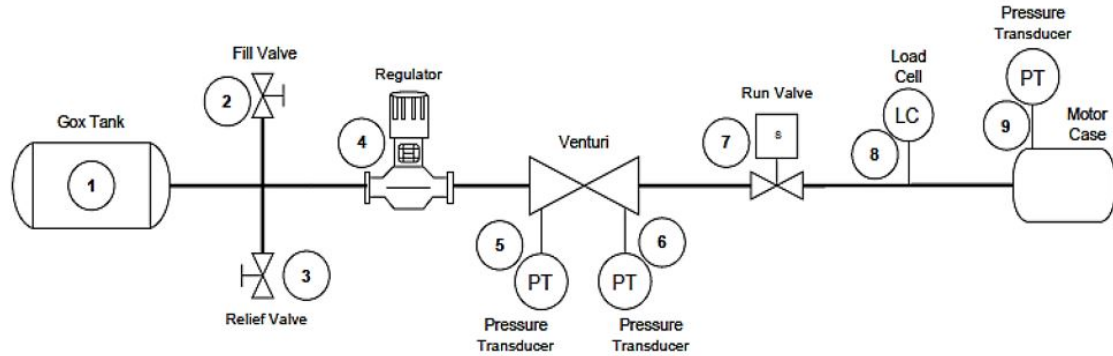

Fig. 4.3: Piping and Instrumentation Diagram of the Ambient Test Apparatus [3]

Figure 4.4 shows the instrumentation deck layout. Figure 4.4a shows the top of the instrumentation deck where there are three NI DAQ units shown; (left to right) USB 6009, USB 6002, USB 9213. The NI USB 6002 is used to read and write data from several bridge transducers and acts as the controller for the high voltage signal using a single TTL-level (3.2-volt) digital command. The NI USB 6009 served as an additional device to read and write data since all the channels on the USB 6009 were used. The NI USB 9213 served as a read and write device for various thermocouple probes inserted in the flow at critical locations to record the temperature of the Nytrox. Figure 4.4b shows the side view of the instrumentation deck. Shown from left to right is the NI 9481 electromechanical relay, HVPS, and power supplies. All data acquisition and control processes were programmed onto a control laptop computer using the LabVIEW® programming language. Communication from the laptop to the instrumentation system was achieved by using a 30-ft amplified USB 2.0 extension cable.

The ignition system power processing unit (PPU) is based on the UltraVolt® D-series line of high-voltage power supplies (HVPS). As previously pictured in Figure 1.2, the HVPS

Table 4.2: Instrumentation List of the Single Motor Tests

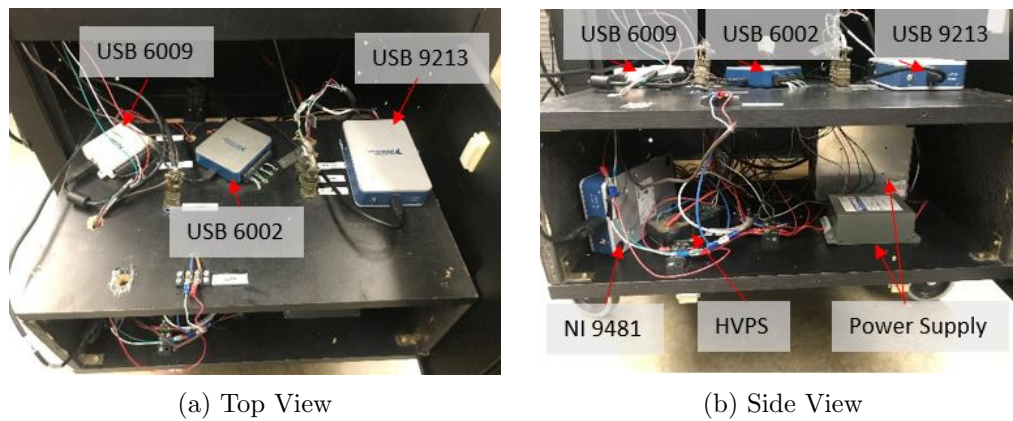| Transducer	
Chamber	Omega PX409-1.0KA5V
Nytrox Bottle	MSP-600-05K-P-4-N-21
Venturi Inlet	Omega PX35D0-500GV
Venturi Throat	PX409-015DDUV
Load Cell	Omega LCCA 25 lbf
Thermocouples	Type K and J

(a) Top View   (b) Side View

Fig. 4.4: Instrumentation Deck Top View and Side View

provides the inductive ignition spark that pyrolyzes sufficient ABS material to seed combustion. The D-series HVPS units take a 15-volt DC input and provide a current-limited (7.5 mA) high voltage output – up to 1000 V or 6 Watts total output. Previous experience with this ignition system has demonstrated that ignition can be reliably achieved using as little as 3 watts. Depending on the impedance on the arc path between the ignitor electrodes, the dissipated voltage typically varies between 10 and 400 volts. Total energy of ignition is typically less than 3 Joules. Ignition energy results will be reported later in this paper.

Directly aft of the thrust chamber lies the solenoid actuated GOX run-valve. The solenoid flow valve is actuated via a digital out command from the instrumentation. The National Instruments USB-6002 initiates "Ignition Control" sending power to the solenoid valve via the solid-state relay and HVPS TTL-level activate signal using the NI 6002 as the

controller. The 24V power supply is used to supply power to the solenoid valve and HVPS; whereas, the 15V power supply is used to power the transducers. The thermocouples, venturi inlet, differential, and chamber pressure transducers, along with the load cell all have their signals conditioned using National Instruments Data Acquisition (DAQ) units.

4.3 Hot Fire Test Procedures

Initially a set of baseline tests was performed using gaseous oxygen as the oxidizer. This test series will ensure that the system has been returned to the status that existed during the testing campaign of Ref. [31]. Key parameters to be measured during this baseline test series include ignition power, thrust, chamber pressure, massflow, fuel regression rate, and specific impulse.

Following the baseline tests, the GOX tank was swapped for the NOS run tank filled with the processed Nytrox. Other than the change in oxidizer, the test assembly will remain identical. For the Nytrox tests, the downstream regulator setting is adjusted to deliver this blended mix at exactly the same chamber pressure as for the GOX tests. Special attention was placed on establishing the required ignition power, and the resulting thrust, specific impulse and fuel regression rates. Tests were performed using the NOS run tank at room temperature; and also with the tank chilled by an Ice-bath to ensure that liquid solution is injected into the motor.

The procedures followed were the same for both GOX baseline and Nytrox Tests. Before the motor was assembled, the fuel grain weight and port diameters at both the top and bottom were recorded. The nozzle throat and exit plane diameters were also logged. Finally, the NOS run tank weight and pressure were logged. Once the pre-test measurements were recorded the motor was assembled. The motor assembly leads were connected to the cart, oxidizer feed line attached, and motor assembly mounted to the test stand. The test stand was then moved to the Blast Lab test area for testing. Inside of the test area, A/C power was then connected to the test stand and connectivity checked using the designated lab test computer. The feed line from either the GOX or the NOS run tank was attached to the thruster systems. The entire feed line was then leak checked to ensure proper connections,

and the regulator for the oxidizer feed pressure was set to 320 psig.

For this test campaign power to the ignition "spark" power was active for a total of two seconds, pre-leading the opening of the oxidizer run valve by 1 second. The oxidizer run valve was pre-programmed to open for a prescribed amount time, and for these tests this time varied from 1 second to more than 4 seconds. The motor would snuff immediately after closure of the run valve. Typically, one fuel grain allows for 8 seconds of burn time, so a typical test series would allow two tests of 4 seconds each on a single fuel grain. Following each burn, the previously described weight and geometry measurements were repeated and logged.

4.4   Nytrox Venturi Calibration

The flow of the two-phase, binary N_2O/O_2 fluid mixture through the venturi flow meter is quite complex and a first-principle flow model has not yet been developed. Thus, a simple calibration procedure was performed in order to measure the discharge coefficient C_d with sufficient accuracy to obtain reasonable Nytrox massflow results. These tests were performed using the Batch 2 Nytrox mixture. A total of 10 cold-flow calibration runs were performed, with the first 5 batches flowing for 2 seconds each and the last 5 flowing for 10 seconds each. The regulator pressure was set to 310 psig, and the oxidizer in the NOS run tank was weighed before and after each burn. The cold flow test apparatus was identical to the previously-described hot flow setup, except that the thrust chamber and fuel grain were removed and the ignition spark was not initiated.

Figure 4.5 plots the cold-flow test results. Plotted are the test data, a linear least squares curve fit, and the curve uncertainties boundaries plotted at the 95% confidence level based on the student-t model [33]. The 5 data points at both the top and bottom ends of the curve are from the cold flow tests performed. The abscissa plots the total integrated massflow over the cold-flow run as predicted by the compressible venturi model, assuming that $C_d = 1.0$. The ordinate plots the actual flowed oxidizer mass measured from the pre-and post-test weights of the NOS run tank. The curve fit coefficients are also noted on this fit. Generally, the fit is rather good with only slight bias of about 2.6 grams,
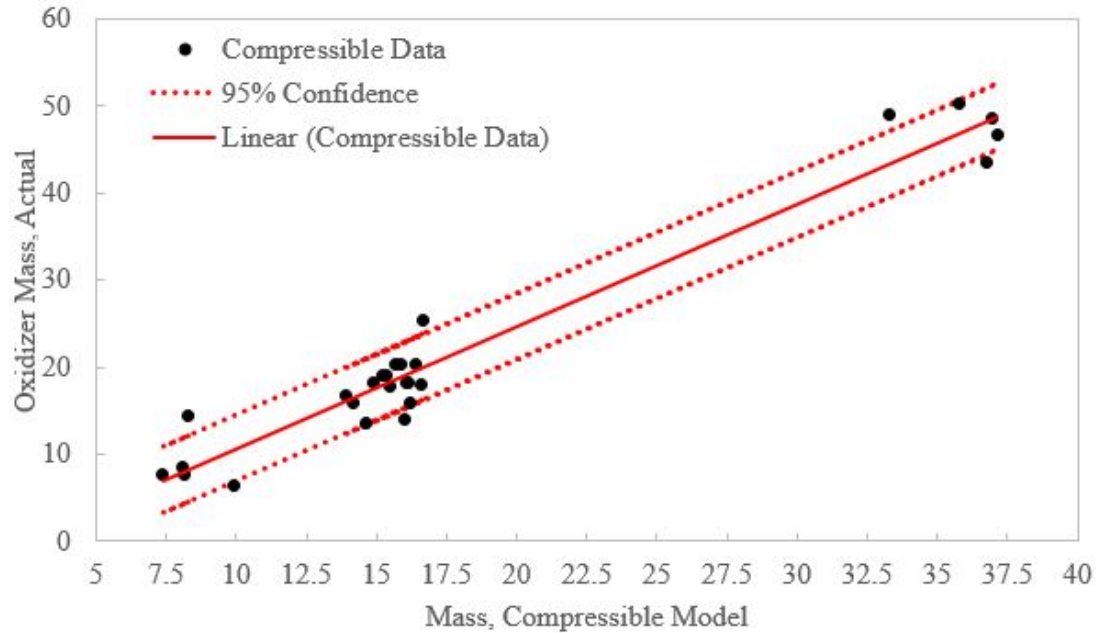
Fig. 4.5: Nytrox Venturi Calibration Data

which is likely due to a tank tare weight error. Interestingly, the curve fit shows a slope (corresponding to the effective discharge coefficient) value at approximately 1.389; a value which is theoretically larger than the maximum possible value of 1.0 for an ideal gas flow. Clearly, there were some un-modeled two-phase effects happening during this flow.

Throughout the testing campaign, the value of C_d was calculated for each hot-fire test performed. These values are also shown on Figure 4.5 and validate the calibration technique and determined value of C_d for the Nytrox testing.

With this method the molecular weight, gas constant, and ratio specific heats were calculated based on the tank ullage vapor composition as shown by Table 2.1, being calculated from the averages of the six Nytrox batches. Pressing forward to the Nytrox Hot-fire testing campaign the following parameters were used for the venturi flow calibration,

- $M_w = 38.625$ g/mol

- $R_g = 215.261$ J/kg-K

- $\gamma = 1.3399$

- $C_d = 1.38915$

It can be noted that the value of C_d presented in this section is different from the value used in the Nytrox/ABS Model presented in Section 3.4. This is due to the Nytrox/ABS Thruster Model using equations that assume an incompressible massflow, which, due to the two-phase flow, is incorrect during testing. The effect of the two-phase flow would drop the choking massflow. It is assumed that the flow is chocked at the injector so an equivalent incompressible value of C_d can be calculated to be 0.65.

CHAPTER 5

RESULTS AND DISCUSSION

The results of the previously described testing campaign are presented in this section. The results from sixteen successful tests are presented. Of those tests, 13 hot-fire burns used GOX as the oxidizer, six 2 second burns and seven 4 second burns, and 17 hot fire burns swapped out Nytrox for GOX, each burn lasting 4 seconds. The GOX results established the system baseline. Results from the GOX and Nytrox burn tests will be presented individually and then compared.

Both venturi flow meters were calibrated using cold flow tests that captured the total mass passed through the system. Previously Bulcher [31] and Whitmore [32], performed extensive cold flow tests and measured the discharge coefficient for GOX flow to be approximately 0.95. Since the test setup for the GOX baseline tests did not change from the original tests of Refs. [31] and [32], the venturi was not calibrated using cold GOX flow for this campaign

For testing purposes the regulator pressure and injector port diameter were pre-set to choke the injector flow and ensure a constant oxidizer mass flow. Choking the injector flow ensured very low run-to-run variability in the oxidizer massflow rate, and significantly reduced the risk of incurring injector-feed coupling instabilities during combustion.

Each fuel grain was burned multiple times to allow interim fuel mass consumption measurements between burns.

The calculations of Equations 3.3-3.10 were iterated, adjusting η^* until the calculated fuel mass equals the measured mass and total consumed propellant O/F ($\Delta M_{ox}/\Delta M_{fuel}$) within a prescribed level of accuracy (0.5%).

The thrust coefficient C_F and specific impulse I_{sp} were also calculated from the thrust values sensed by the test stand load cell. The values calculated by Eqs. 3.23 and 3.24 provide

redundant measures, and will be presented later in order to support the verisimilitude of the collected test data.

5.1 GOX/ABS Test Results

(a) Specific Impulse vs. O/F Ratio

(b) Characteristic Velocity vs. O/F Ratio

(c) Thrust Coefficient vs. O/F Ratio
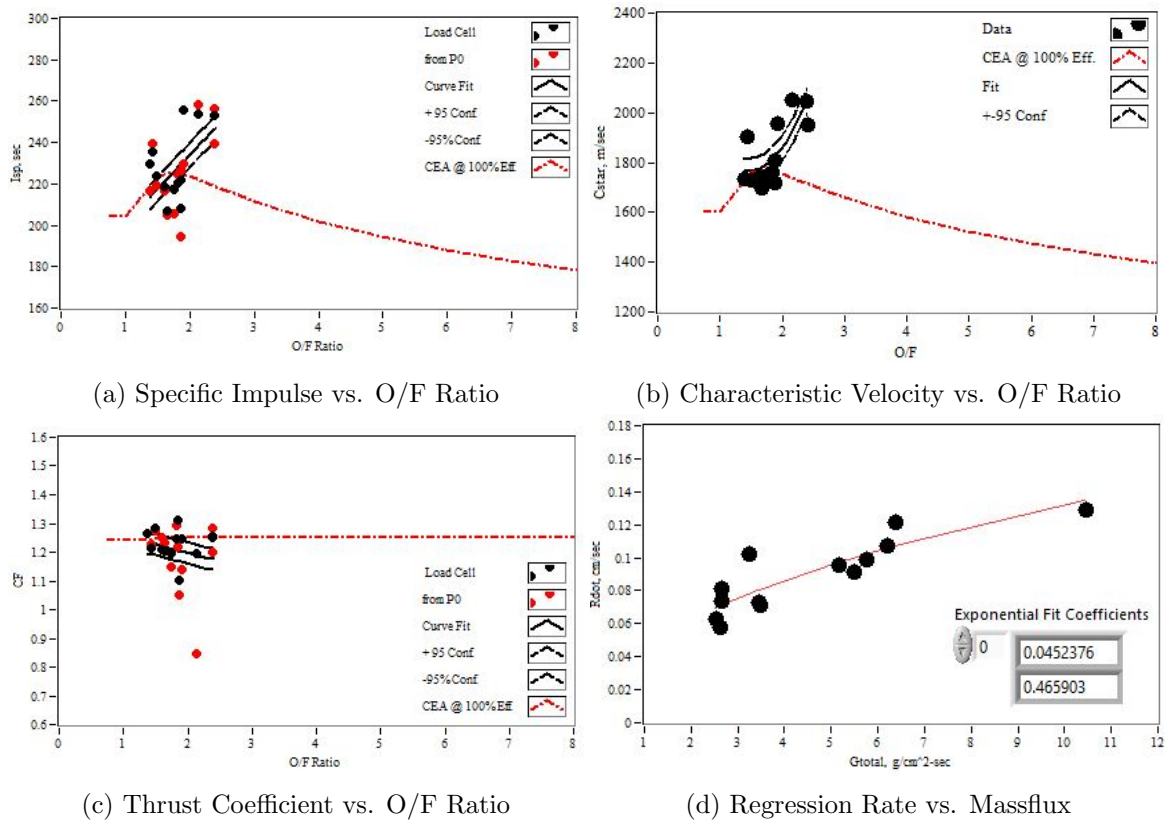

(d) Regression Rate vs. Massflux

Fig. 5.1: Summary of the GOX/ABS Baseline Test Results

To determine a baseline of which to compare performance metrics for future Nytrox burns a series of GOX burns were completed. Figure 5.1 summarizes the baseline test results. Plotted are I_{sp}, c^*, C_F, and the mean ABS fuel regression rate $\dot{r}$. The fuel regression rate is plotted as a function of total massflux G_{total}. The specific impulse and thrust coefficient curves plot values calculated using both the sensed thrust from the load cell, and the thrust calculated from chamber pressure using the method described in the previous section. The expected values calculated from CEA (Ref. [19]) assuming 100% combustion efficiency and

frozen flow at the nozzle throat are also overlaid on the are I_{sp}, C_F, and c^* plots. The plotted data are generally supported by the theoretical calculations. On Figure 5.1b it is shown that the thruster is operating in the optimal O/F range, this result is mimicked in Figure 5.1a. Additionally, the values shown by Figure 5.1 agree with results previously published by refs. Refs. [31] and [32], and these results support the hypothesis that the reassembled test article and test stand was returned to its previous state of performance, for which there is an extensive data base.

It needs to be noted that the test data shows slightly higher values than the prediced 100% CEA model values on Figure 5.1a and 5.1b. This is due to inefficiences with the chamber pressure transducer measurement that started occuring part way through the testing campaign. The issues with the chamber pressure measurement are addressed in Section 7.2 with possible solutions presented. However, any issues with the chamber pressure measurements were very small, fixing the issue will only validate the gathered data in this thesis and increase the fidelity of the data.
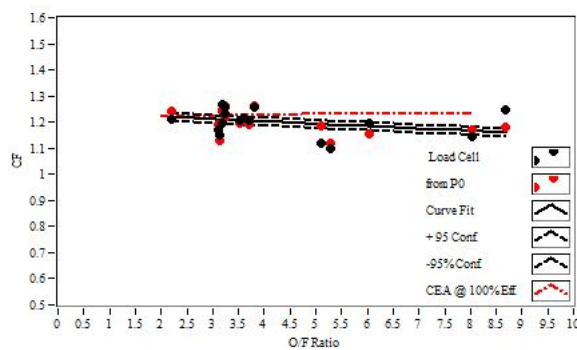
5.2 Nytrox/ABS Test Results

Figure 5.2 summarizes the results of the 16 Nytrox hot fire tests. The Nytrox mixture used for these tests was Batch 6, with the mixture properties listed by Table 2.1. As with the previous plots of the GOX/ABS baseline data, Figure 5.2a plots I_{sp}, Figure 5.2b plots c^*, Figure 5.2c plots C_F, and Figure 5.2d plots the mean ABS fuel regression rate plotted as a function of G_{total}. The corresponding CEA curves assuming a Nytrox 88 (88% N_2O) liquid composition are also plotted. Here there is significantly more scatter exhibited by the data, a likely result of the massflow uncertainty as calculated by the venturi flow meter, and the variability of the Nytrox fluid composition as the tank empties. As expected from the theoretical comparisons of Figure 3.1 the mean I_{sp} and c^* values are approximately 10% lower, due to the reduced flame temperature associated with Nytrox combustion. When using Nytrox as a "drop in" replacement for GOX, the motor tends to run slightly richer than the O/F value required for optimal performance. Since the thruster fuel grain had been previously optimized for best O/F ratio based on GOX as the oxidizer, this was not
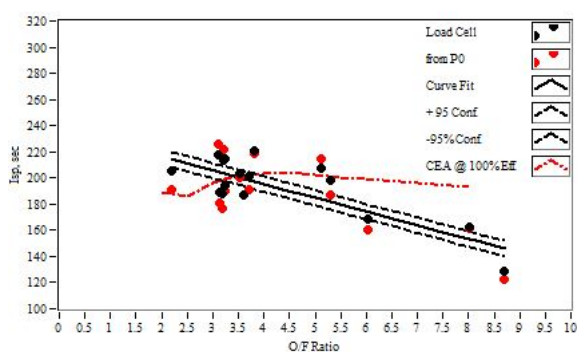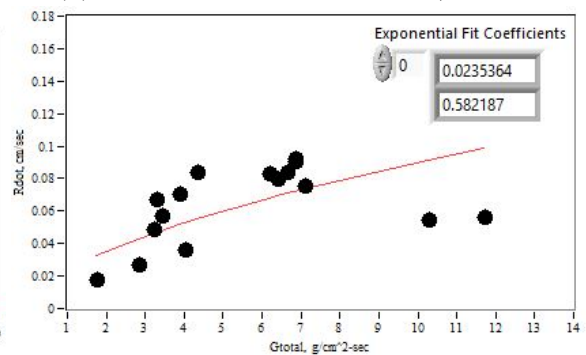
(a) Specific Impulse vs. O/F Ratio
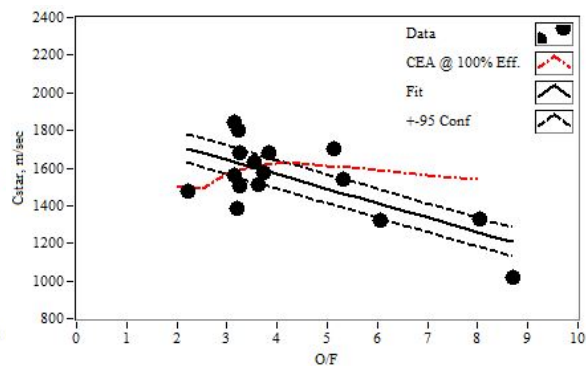
(b) Characteristic Velocity vs. O/F Ratio

(c) Thrust Coefficient vs. O/F Ratio

(d) Regression Rate vs. Massflux

Fig. 5.2: Summary of the Nytrox/ABS Test Results

surprising. The mean Nytrox combustion efficiency, calculated for each burn as the ratio of the measured c* to the theoretical value as predicted by CEA was 96.14%.
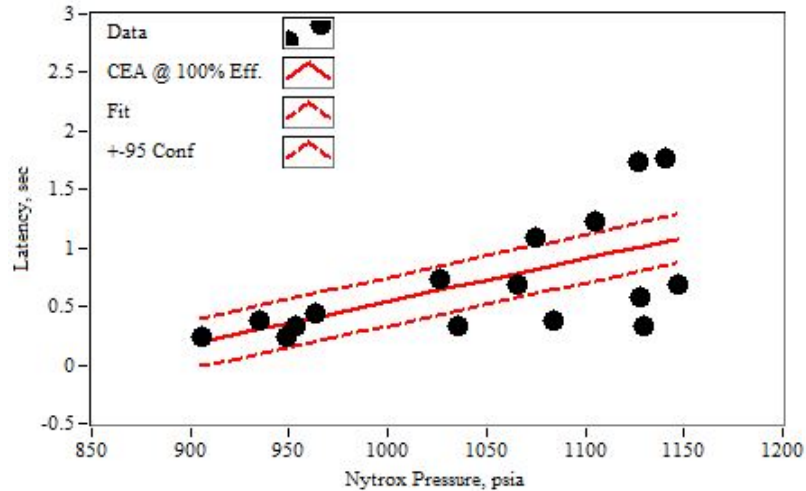

Fig. 5.3: Ignition Latency vs Nytrox Tank Pressure

Throughout the testing campaign a slight latency in motor ignition time was noticed in the physical burns as well as the data recorded. It was noted that the ignition latency seemed greater as the tank warmed up due to sitting outside of the freezer during testing. The tank pressure is directly correlated to the tank temperature. The tank pressure was then plotted against the ignition latency from the data, shown in Fig. 5.3. This validates the correlation of ignition latency with tank pressure for Nytrox. Therefore, the colder the Nytrox mixture becomes the faster the motor ignites.

It is noted that the overall spread of the data for the Nytrox/ABS testing is larger compared to the GOX/ABS testing. This is due to eight of the hot-fire tests have a larger injector port diameter. This change was done to investigate the effect that would occur. By increasing the injector port diameter it resulted in a larger O/F during the burn and a lower regression rate of the fuel grain.

5.3 Data Comparisons

To best compare the data from the baseline GOX test campaign and the Nytrox test

campaign, the mean values of I_{sp}, c^*, C_F, O/F, and energy required for ignition are calculated and shown side-by-side in a bar graph. Included in the bar graphs are error bars calculated assuming a student-t distribution and a 95% confidence level. The regression rate curves for each oxidizer are then compared on the same graph along with other common oxidizer fuel combinations for hybrid thrusters.

As shown in Figures 5.4a and 5.4b the Nytrox produces lower levels of specific impulse and characteristic velocity, respectively. This was expected from the results shown in Figure 3.1. Both systems, however, acheived nearly identical levels of thrust coefficient, as shown by Figure 5.4c. This was unsurprising due to chamber pressure levels being nearly identical for each system as well. This was achieved by tuning the feed pressure into the system using a pressure regulator located upstream of the motor. The purpose of striving for nearly identical chamber pressure levels was to collect better performance metrics of the motor by keeping as many variables as possible constant during both testing campaigns.

The ignition energy required for each oxidizer remained at relatively the same level, $2 - 2.5J$, for each oxidizer. This shows great promise for future use in the small satellite market. By requiring such small levels of energy for ignition more energy can be focused on instruments vital to the success of the mission.

From Figure 5.4d it is shown that the Nytrox produces a larger mean O/F. Again, this was expected from the results of Figure 3.1. However, to better analyze the O/F ratios produced by each oxidizer the equivalence ratios must be compared. This process is shown in Eq. 3.16. The Nytrox/ABS thruster operated at $\Phi = 1.5414$, whereas the GOX/ABS thruster operated at $\Phi = 1.5452$. A difference of less then 0.25%. This shows, once again, that the thrusters were nearly identical in performance.

The equivalence ratio is an important metric because generally, ABS burned as a hybrid rocket fuel tends to have a higher overall performance when burned at an equivalence ratio Φ that lies between 1.5 and 2.0. By burning at fuel rich equivalence ratios, there are several benefits, namely, the effect of reducing the flame temperature, lowering nozzle throat erosion, and producing a plume with a lower molecular weight composition. Both thrusters

(a) Specific Impulse

(b) Characteristic Velocity

(c) Thrust Coefficient
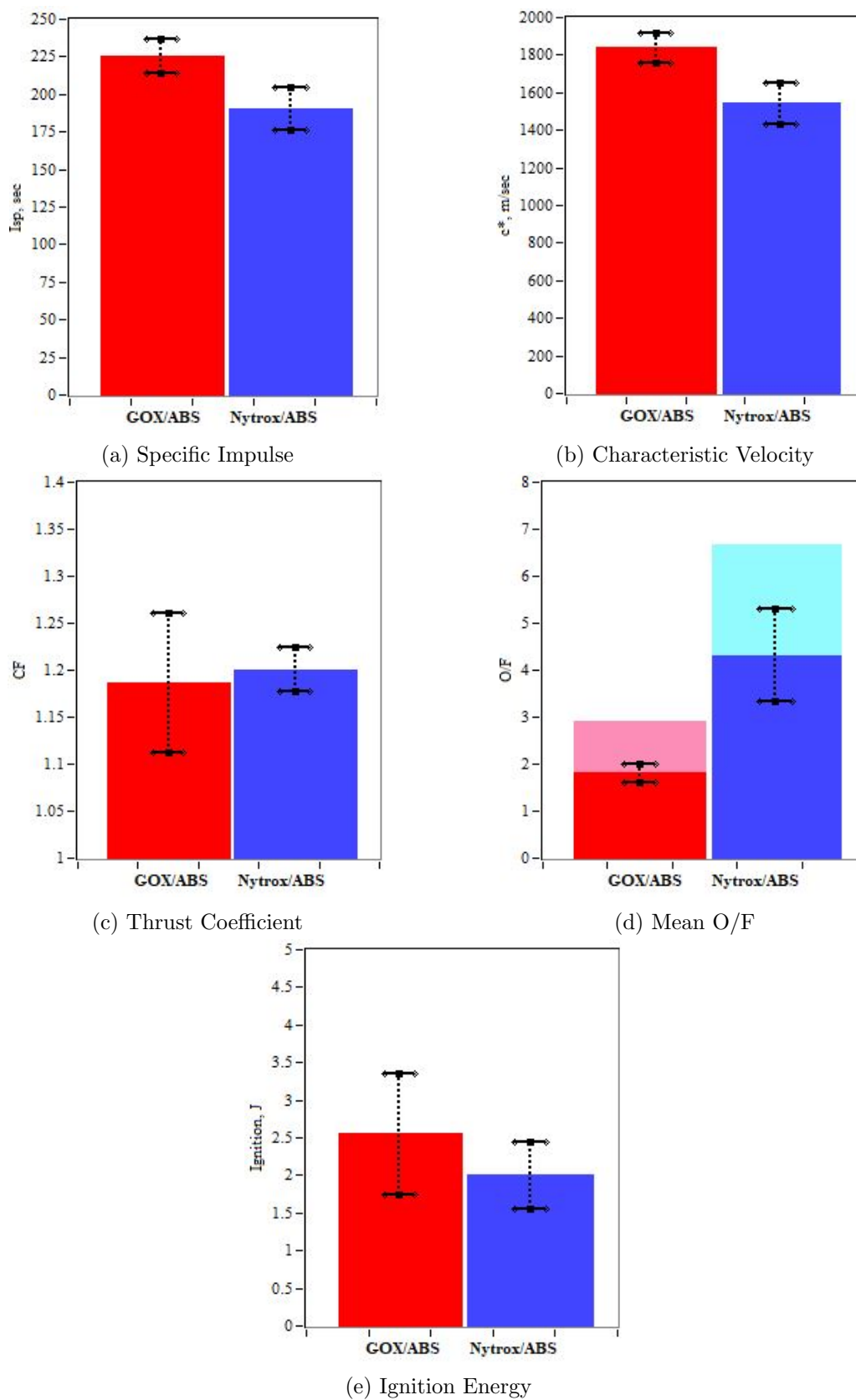

(d) Mean O/F

(e) Ignition Energy

Fig. 5.4: Bar Graphs Showing Comparing Results of Nytrox and GOX Test Campaigns

operated in this fuel rich zone.

Since both motors produce equivalent levels of thrust and chamber pressure, but the Nytrox/ABS contains a larger O/F, the regression rate must be analyzed to more fully understand the difference between the motors.
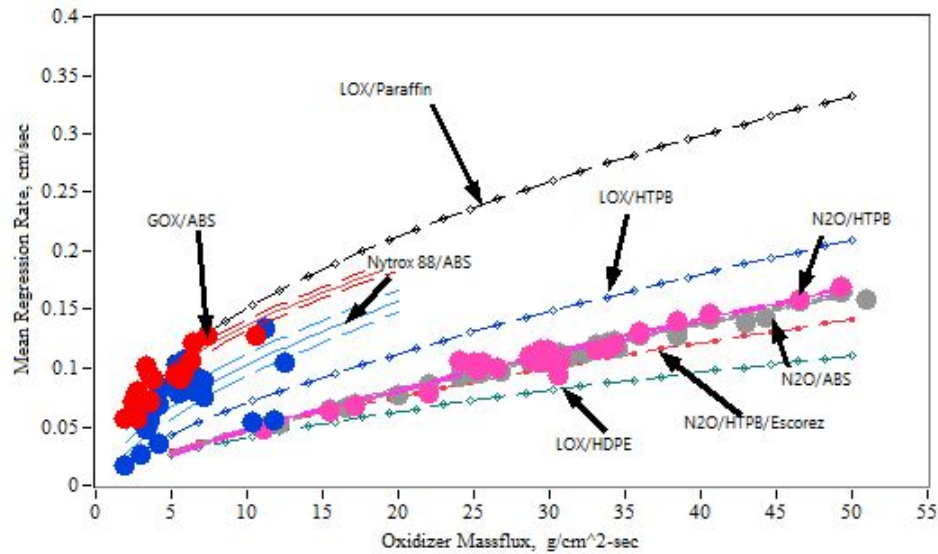

Fig. 5.5: Regression Rate Comparisons

Figure 5.5 shows the regression rate of both GOX/ABS and Nytrox/ABS, along with several other common hybrid thruster oxidizer fuel combinations. The Nytrox/ABS regression rate is slightly lower than the GOX/ABS regression rate, however, both outperform almost every other common combination used in hybrid thrusters. Therefore, the Nytrox/ABS thruster matches the GOX/ABS thruster in thrust by having a lower regression rate in the fuel and a higher mean O/F level.

Although both the Nytrox/ABS and GOX/ABS thruster produce nearly identical performance metrics, the benefit of using Nytrox as a drop-in for GOX lies in the density specific impulse, $\rho \cdot I_{sp}$. The Nytrox/ABS propellants exhibit a higher density specific impulse, approximately 1075 N-s/liter compared to the 1036 N-s/liter for GOX/ABS baseline propellant. This calculation is based upon the oxidizer storage density, and not the downstream flow density. For this calculation the GOX is assumed to be stored at 2000 psig,

and at 288°C, with the resulting storage density of approximately $0.185g/cm^3$. The Nytrox storage density is taken from the average of all the batches from Table 2.1 or approximately $0.422g/cm^3$. Also, note that this relatively low Nytrox storage density results from the NOS run tank only being half-filled (5 lbs.) with nitrous oxide during processing. If the tank were filled closer to capacity with nitrous oxide, the density specific impulse of the Nytrox will continue to grow even more rapid compared to the GOX.

5.4 Comparison To Other Oxidizers

In order to compare the performance of Nytrox/ABS against existing space mono-propellants, such as hydrazine, the performance metrics calculated must be extrapolated to space environment conditions. Recall that the specific impulse and density-impulse values plotted on Figure 5.4 were derived from data collected under ambient test conditions at approximately 1,430 meters (4700 ft.) altitude, the elevation of the PRL test facility in Logan, Utah. The 2.07 expansion-ratio nozzle was designed to give optimal performance at this altitude. When matched with a high expansion-ratio nozzle, the vacuum performance will be significantly better. This data can be extrapolated to altitude by using the previously presented 1-D de Laval flow equations from Eqs. 3.19 - 3.27. Using this model, the specific impulse under optimal conditions can be written in terms of the optimal thrust coefficient and the nozzle exit-to-chamber pressure ratio.

The thrust coefficient is

$$(C_{F_{vac}})_{test} = \gamma \cdot \sqrt{\frac{2}{\gamma-1}\left(\frac{2}{\gamma+1}\right)^{\frac{\gamma+1}{\gamma-1}} \cdot \left(1 - \frac{P_{exit}}{P_0}\right)^{\frac{\gamma-1}{\gamma}}} + \frac{A_{exit}}{A^*}\left(\frac{P_{exit} - P_\infty}{P_0}\right) \quad (5.1)$$

$$(C_{F_{vac}})_{opt} = \gamma \cdot \sqrt{\frac{2}{\gamma-1}\left(\frac{2}{\gamma+1}\right)^{\frac{\gamma+1}{\gamma-1}} \cdot \left(1 - \frac{P_{exit}}{P_0}\right)^{\frac{\gamma-1}{\gamma}}} \quad (5.2)$$

Using C_F to scale specific impulse results in

$$\frac{(I_{sp})_{opt}}{(I_{sp})_{test}} = \frac{\frac{P_0 \cdot A^*}{g_0 \cdot \dot{m}}\left(C_{F_{opt}}\right)}{\frac{P_0 \cdot A^*}{g_0 \cdot \dot{m}}\left(C_{F_{test}}\right)} = \frac{\gamma \cdot \sqrt{\frac{2}{\gamma-1}\left(\frac{2}{\gamma+1}\right)^{\frac{\gamma+1}{\gamma-1}} \cdot \left(1 - \frac{(P_\infty)_{vac}}{P_0}\right)^{\frac{\gamma-1}{\gamma}}}}{\gamma \cdot \sqrt{\frac{2}{\gamma-1}\left(\frac{2}{\gamma+1}\right)^{\frac{\gamma+1}{\gamma-1}} \cdot \left(1 - \frac{(P_{exit})_{test}}{P_0}\right)^{\frac{\gamma-1}{\gamma}}} + \left(\frac{A_{exit}}{A^*}\right)_{test}\left(\frac{(P_{exit})_{test} - P_\infty}{P_0}\right)}$$
$$(5.3)$$

Using the motor parameters, thrust coefficient, mean chamber pressure, and the CEA-derived Thermochemistry Parameters for Nytrox 88/ABS, and assuming a 96.14% combustion efficiency (from Section 5.2). Figure 5.6 plots this extrapolation. Figure 5.6a shows the optimal expansion ratio for the Nytrox 88/ABS motor as a function of altitude, Figure 5.6b plots the optimal C_F as a function of expansion ratio, and Figure 5.6c plots the optimal specific impulse as a function of expansion ratio. Also plotted as the black symbols are the actual values for the Nytrox 88/ABS motor. Note at an expansion ratio of 50, corresponding to an altitude of 29 km (95,000 ft.) the optimal C_F exceeds 1.8 and the optimal I_{sp} reaches a value of approximately 295 s.

Using these extrapolated results a comparison of Nytrox to hydrazine, LMP-103S, and AF-M315E, can now be done. Table 5.1 shows multiple metrics for each oxidizer. Data for hydrazine, LMP-103S, and AF-M315E were taken from Ref. [31]. Nytrox does have the largest flame temperature, but this is due to the high pyrolysis energy that ABS fuel possesses. Because ABS hybrid motors are self-ablative the external surfaces do not reach these high temperatures. Nytrox delivers a specific impulse of nearly 300 s in a vacuum
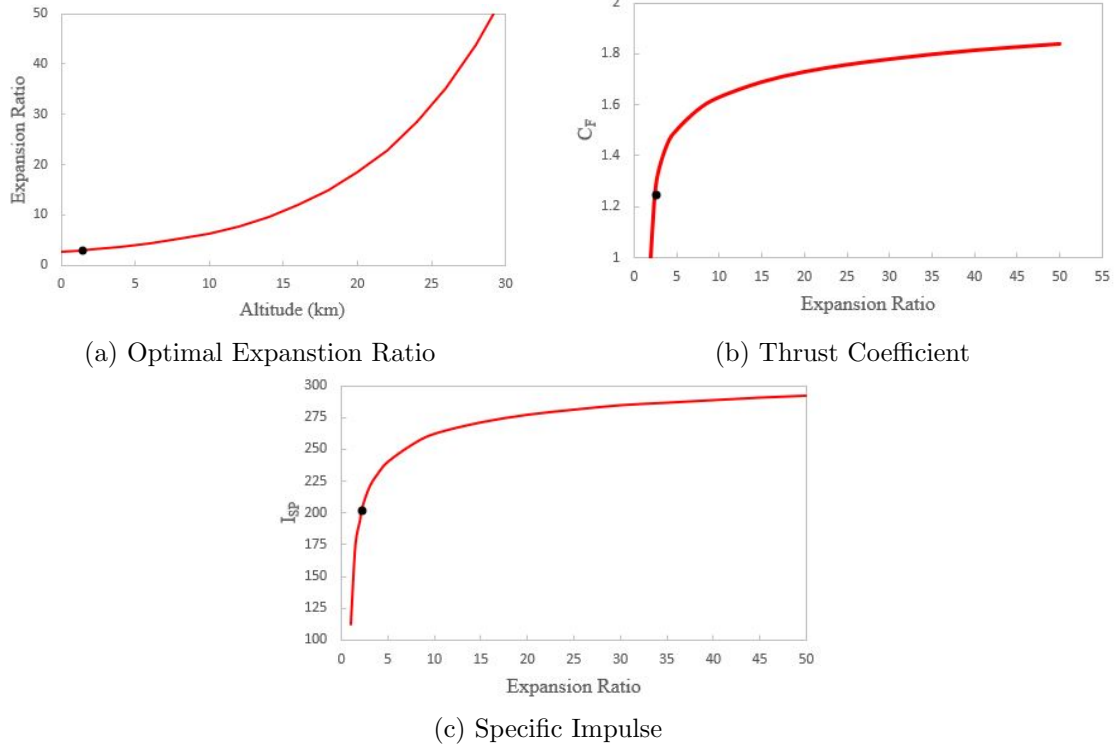
(a) Optimal Expanstion Ratio

(b) Thrust Coefficient

(c) Specific Impulse

Fig. 5.6: Extrapolating Test Results to Optimal High Altitude Conditions [3]

environment, extrapolated to vacuum conditions from ground test data, this value is more than 25% higher than can be achieved by any of the "green" ionic liquid propellants or mono-propellant hydrazine. Using the 295 s I_{sp} value to extrapolate the $\rho \cdot I_{sp}$, the projected vacuum value rises to approximately 1920 N-s/liter.

For Nytrox there is no preheat temperature needed before ignition, and the ignition energy required is only 2-5 J for 500 ms. This value trumps the other propellants which require 10,000+ J for 600+ s. Allowing more energy to be used by sensors on the spacecraft for mission success. Nytrox is also very widely available, 80-90% N_2O solutions are easily manufactured, as per the procedure outlined in Section 2.2. With the exception of density impulse, the Nytrox/ABS system outperforms the other propellants in every measurable category. However, because Nytrox had the ability to safely self-pressurize, there is no need for an additional pressurant tank in the system to maintain workable pressure levels in the Nytrox tank. Thus, even in terms of volumetric efficiency, Nytrox 88/ABS appears to have a definite advantage.

Table 5.1: Comparison of Nytrox/ABS Performance Characteristics to Existing Space Mono-Propellants [3]

Propellant	Hydrazine	LMP-103S	AF-M315E	Nytrox/ABS Hybrid
Flame Temperature (°C)	600-750	1600	1900	3000
I_{sp} (s)	220-225	252 (theory) 235 (actual)	266 (theory) 245 (actual)	300 (theory) 294 (actual)
Specific Gravity	1.01	1.24	1.465	0.65
Density Impulse (N-s/L)	2270	3125 (theory) 2915 (actual)	3900 (theory) 3650 (actual)	2000 (theory) 1900 (actual)
Preheat Temperature (°C)	315, cold start capable	300	370	N/A none required
Required Ignition Input Energy (J)	10,000 J (10 Watts for 600 s)	12,000 J (10 Watts for 1200 s)	27,000 J (15 Watts for 1800 s)	2-5 J (4-10 Watts for 500 ms)
Propellant Freezing Temperature (°C)	1--2	-7	< 0 (forms glass, no freezing point)	-70
Cost	$	$$$	$$$$	$
Availability	Readily Available	Restricted Access	Limited Access	Very Widely Available
NFPA 704 Hazard Class	Health 4, Flammability 4, Reactivity 3	Health 1, Flammability 0, Reactivity 4, OXY	Health 1, Flammability 0, Reactivity 3, OXY	Health 3, Flammability 0, Reactivity 0, OXY

CHAPTER 6

SUMMARY AND CONCLUSION

In recent years, the PRL has successfully developed a promising High Performance Green Hybrid Propellant using non-toxic oxidizers and 3-D printed fuel. This thruster utilizes the arc-ignition system developed at USU, and has had successful tests in a vacuum environment on a sounding rocket launched in March 2018. This thesis investigated the feasibility of mixtures of N_2O and O_2, commonly known as Nytrox, as a drop-in replacement for GOX.

Nytrox provides a greater density and specific gravity than GOX alone, while also providing a higher specific impulse than N_2O alone. By adding O_2 to the N_2O it lowers the optimal O/F and significantly mitigates the possibility of the N_2O vapor rapidly decomposing and exploding. Nytrox is a self-pressuring oxidizer blend, thus reducing the overall system complexity. The performance metrics of Nytrox were first analyzed through NASA's CEA program.The Peng-Robinson two-phase binary solution model was used as guidance for developing the correct mixing procedure. A series of six Nytrox mixtures were then successfully made, using the procedure described in Section 2.2, throughout the duration of this thesis campaign with results shown in Table 2.1.

A series of 13 hot-fire tests were first completed using GOX as the oxidizer. These tests were used to verify working condition of the test cart and calibration of sensors used for measuring temperature and pressure at several locations along the flow path. The GOX was then swapped out for the Nytrox, with no other changes made to the test stand. With the Nytrox installed, a series of 16 hot-fire tests were then completed. Using data collected from three NI data aquisition units, each burn was analyzed and performance metrics were calculated for I_{sp}, c^*, C_F, and $\dot{r}$. Comparing the results from each oxidizer showed results matching the CEA model, namely, GOX providing a larger I_{sp} and c^*, but Nytrox having a larger O/F ratio. Further analysis showed that both oxidizers had approximately the

same C_F and ignition energy. These results are shown in the bar graphs of Figure 5.4. The regression rate of each oxidizer with ABS fuel was then compared to each other and several other common hybrid thruster systems. Figure 5.5 shows this comparison and it is to be noted that while GOX/ABS has the higher regression rate compared to Nytrox/ABS, the Nytrox/ABS regression rate is significantly larger than all other common hybrid thruster systems except LOX/Paraffin.

The results from the Nytrox/ABS testing were extrapolated to vacuum conditions and compared to hydrazine, and the "promising" ionic liquid propellants LMP-103S and AF-M315E, shown on Table 5.1. From Table 5.1 it can be seen that while Nytrox/ABS has a lower density impulse, compared to the other three propellants, it out performs in every other catagory. But due to Nytrox being a self-pressuring oxidizer, it does not require a separate pressurant tank to maintain workable pressures during use. With this in mind, it consequently would provide a larger density impulse, and proves that it is the greater propellant.

Since this is one of the first testing campaigns done using Nytrox as a hybrid thruster oxidizer, more testing needs to be done to fully optimize the system. A few points of emphasis for further testing are outlined in Chapter 7. But with the progress made thus far and analysis of the data, it has been shown that Nytrox out performs common mono-propellants and most common hybrid thruster combinations. In the end, it can be stated that this thesis project was successful in the goal of developing Nytrox as a viable drop-in replacement for GOX.

CHAPTER 7

FUTURE WORK

This chapter will briefly outline three points of interest for future testing campaigns to be completed. This is not a comprehensive list of all points for future work, but from these points a greater understanding of Nytrox will be developed and will inevitably lead to further points of future work to be completed.

7.1 Nytrox Ignition Latency

During the hot-fire testing of the GOX/ABS thruster, it was noted visually as well as in the data collected that the thruster fully ignited almost instantly when the oxidizer began flowing into the motor. This is shown by the load cell measurement in Figure 7.1, where the solenoid valve opens and GOX begins to flow into the ignition chamber at $t = 0s$.
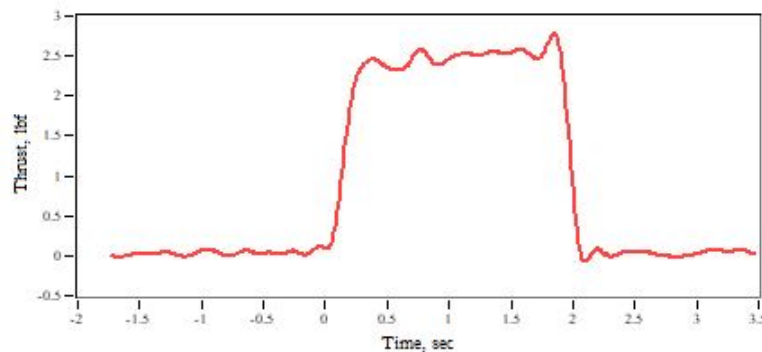

Fig. 7.1: Example of GOX/ABS Burn Chamber Pressure Time History

However, with the Nytrox/ABS thruster there were ignition latencies of up to 500 ms before the thruster was fully ignited. A load cell measurement time history is shown in Figure 7.2, again the solenoid valve opens and Nytrox begins to flow at $t = 0s$. The latency was discussed in Section 5.2.

A very strong correlation was seen in Figure 5.3 that as the temperature of the oxidizer
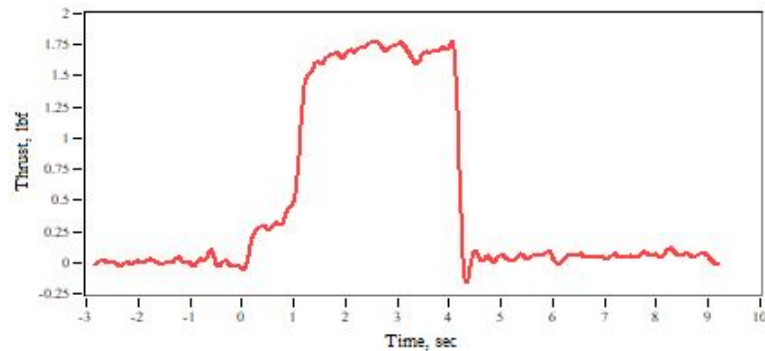
Fig. 7.2: An Extreme Example of Nytrox/ABS Burn Load Cell Time History

was reduced, resulting in the reduction of pressure of the oxidizer tank, the ignition latency was also reduced. It is proposed that further research be done on this phenomenon. Perhaps cooling the nytrox down even further or allowing it to warm up slightly more than room temperature. By performing hot-fire tests at a larger variety of Nytrox tank temperatures, the graph of Figure 5.3 can be more fully populated with data points.

7.2   Chamber Pressure Transducer Inefficiencies

At the beginning of testing for this thesis research the chamber pressure transducer measurement looked very sharp and similar to chamber pressure data profiles seen in the past on other research projects. However, throughout testing this sharp profile became more sloped. During both the GOX and Nytrox hot-fire testing campaigns the pressure transducer calibration was repeated to ensure the correct calibration was being used during testing. Each time the transducer was calibrated it yielded nearly identical results indicating that the calibration was correct. The expected chamber pressure data profile is shown as the green line on Figure 7.3, with the red line being the actual measured chamber pressure profile.

Due to the calibration remaining correct, with the shape of the profile of the data, it is hypothesized that there is a small leak in the chamber pressure caused from it being used for numerous hot-fire burns with several different research campaigns. Therefore, it is proposed that a replacement pressure transducer be calibrated and swapped out for the
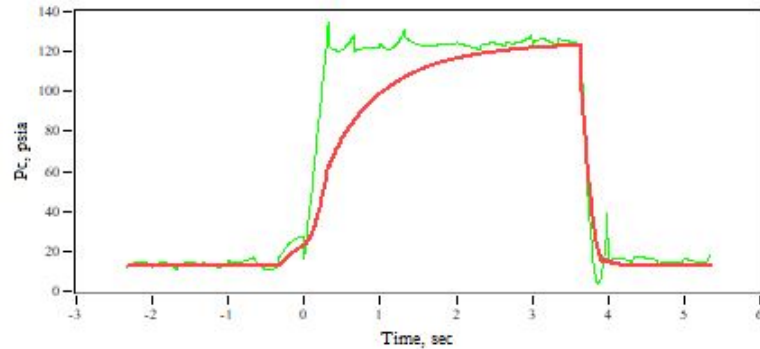
Fig. 7.3: Example of Chamber Pressure Time History Discrepancy

defective transducer before further testing is attempted. This will verify that a leak exists with the current transducer and correct the discrepancy in the expected and actual chamber pressure data profiles.

7.3   Nytrox Optimized Nozzle

From Section 5.2 on Figures 5.2a and 5.2b it can be seen that the cluster of containing the majority of the data points lie slightly below the CEA 100% Efficiency line, shown as the dotted red line. This is due to the nozzle configuration, which was designed and optimized for GOX. Since it has been shown that Nytrox/ABS is a viable drop-in replacement for GOX/ABS, for future work it would be beneficial to machine a new graphite nozzle. The new nozzle would be designed and optimized for use in Nytrox/ABS hybrid thruster systems. Doing this would give even better performance from the Nytrox/ABS thruster, thus strengthening the argument of Nytrox being the better propellant.

REFERENCES

[1] "Nfpa." [Online]. Available: https://www.nfpa.org/

[2] "Mil-std-882e." [Online]. Available: https://www.system-safety.org/Documents/MIL-STD-882E.pdf

[3] S. Whitmore, R. Stoddard, R. Babb, and D. Horlacher, *Medical Grade N2O/O2 Mixtures as Inexpensive and Volumetrically Efficient Oxidizers for Small Spacecraft Hybrid Propulsion Systems*. [Online]. Available: https://arc.aiaa.org/doi/abs/10.2514/6.2019-4186

[4] M. Karabeyoglu, "Nitrous oxide and oxygen mixtures (nytrox) as oxidizers for rocket propulsion applications," *Journal of Propulsion and Power*, vol. 30, no. 3, pp. 696–706, 2014. [Online]. Available: https://doi.org/10.2514/1.B34768

[5] G. Sutton and O. Biblarz, *Rocket Propulsion Elements*. John Wiley and Sons, New York, 2001.

[6] V. Bombelli and D. Simon, "Economic Benefits of the use of non-toxic mono-propellants for Spacecraft Applications," *AIAA Paper 2003-4783*, 2003.

[7] Iridium. (2017, June) Hydrazine - toxic for humans, but satellites love it. SpaceX/Iridium NEXT.

[8] Robert A. Braeunig. (2008) Rocket Propellants. online. Rocket and Space Technology. [Online]. Available: http://www.braeunig.us/space/propel.htm

[9] D. Haeseler, V. Bombelli, P. Vuillermoz, R. Lo, T. Marée, and F. Caramelli, "Green propellant propulsion concepts for space transportation and technology development needs," vol. 557, p. 4, 09 2004.

[10] M. Y. N., J. I. S. O., A. M. K., and R. d. C. L. D., "Adn - the new oxidizer around the corner for an environmentally friendly smokeless propellant," *Journal of Aerospace Technology and Management*, vol. 1, pp. 153–160, 2009.

[11] A. L. Rheingold, J. T. Cronin, T. B. Brill, and F. K. Ross, "Structure of hydroxylammonium nitrate (han) and the deuterium homolog," *Acta Crystallographica Section C*, vol. 43, no. 3, pp. 402–404, 1987.

[12] Tracy McMahan. (2015, Sept) New Green Propellants complete Milestones. online. NASA. [Online]. Available: https://www.nasa.gov/centers/marshall/news/news/releases/2015/new-green-propellants-complete-milestones.html

[13] R. Masse, M. Allen, R. Spores, E. A. Driscoll, L. Arrington, S. Schneider, and T. Vasek, "Af-m315e propulsion system advances and improvements," *52nd AIAA/SAE/ASEE Joint Propulsion Conference*, Jul 2016.

[14] R. A. Spores, R. Masse, S. Kimbrel, and C. McLean, "Gpim af-m315e propulsion system," *50th AIAA/SAE/ASEE Joint Propulsion Conference*, Jul 2014.

[15] T. McMahan, "Nasa thrusters propelled by new green propellants complete milestones," Sep 2015. [Online]. Available: https://scitechdaily.com/nasa-thrusters-propelled-by-new-green-propellants-complete-milestones/

[16] "Green propellant." [Online]. Available: https://www.federallabs.org/successes/awards/awards-gallery/2018/green-propellant

[17] "Hazard analysis of commercial space transportation; vol. 1: Operations, vol. 2: Hazards, vol. 3: Risk analysis," May 1988. [Online]. Available: https://www.faa.gov/about/office_org/headquarters_offices/ast/.../hazard.pdf

[18] "Department of defense interface standard, eletromagnetic environmental effects requirements for systems, mil-std-464," Mar 1997. [Online]. Available: http://www.tscm.com/MIL-STD-464.pdf

[19] "Computer program for calculation complex chemical equilibrium compositions and applications," Oct 1994. [Online]. Available: https://ntrs.nasa.gov/archive/nasa/casi.ntrs.nasa.gov/19950013764.pdf

[20] "Liquid oxygen," May 2017. [Online]. Available: http://www.airproducts.com/~/media/Files/PDF/company/safetygram-6.pdf

[21] "Occupational safety and health guideline for nitrous oxide." [Online]. Available: http://www.osha.gov/SLTC/healthguidelines/nitrousoxide/recognition.html

[22] D.-Y. Peng and D. Robinson, "A new two constant equation of state," *Industrial and Engineering Chemistry Fundamentals*, vol. 15, no. 1, pp. 59–64, 1976. [Online]. Available: https://doi.org/10.1021/i160057a011

[23] D. Zudkevitch and J. Joffe, "Correlation and prediction of vapor- liquid equilibria with the redlich-kwong equation of state," *AIChE Journal*, vol. 16, no. 1, pp. 112–119, 1970. [Online]. Available: https://doi.org/10.1002/aic.690160122

[24] J. Anderson, *Modern Compressible Flow*, 3rd ed. New York: The McGraw Hill Companies, Inc., 2003. [Online]. Available: https://libcat.lib.usu.edu/search/i0070016542

[25] G. Zilliac and M. A. Karabeyoglu, "Modeling of propellant tank pressurization," *41st AIAA/ASME/SAE/ASEE Joint Propulsion Conference and Exhibit*, pp. 1–25, 2005. [Online]. Available: https://doi.org/10.2514/6.2005-3549

[26] J. Dyer, E. Doran, Z. Dunn, and K. Lohner, "Modeling feed system flow physics for self-pressuring propellants," *43rd AIAA/ASME/ SAE/ASEE Joint Propulsion Conference and Exhibit*, July 2007. [Online]. Available: https://doi.org/10.2514/6.2007-5702

[27] S. A. Whitmore and S. N. Chandler, "Engineering model for self-pressurizing saturated-n2o-propellant feed systems," *Journal of Propulsion and Power*, vol. 26, no. 4, pp. 706–714, July-August 2010. [Online]. Available: https://doi.org/10.2514/1.47131

[28] J. E. Zimmerman, B. S. Waxman, B. J. Cantwell, and G. Zilliac, "Review and evaluation of models for self-pressurizing propellant tank dynamics," *49th AIAA/ASME/SAE/ASEE Joint Propulsion Conference and Exhibit*, July 2013. [Online]. Available: https://doi.org/10.2514/6.2013-4045

[29] B. S. Waxman, J. E. Zimmerman, B. J. Cantwell, and G. G. Zilliac, "Mass flow rate characterization of injectors for use with self-pressurizing oxidizers in hybrid rockets," *60th JANNAF Propulsion Meeting*, 2013.

[30] S. Whitmore, Z. W. A. Peterson, and S. D. Eilers, "Comparing hydroxyl terminated polybutadiene and acrylonitrile butadiene styrene as hybrid rocket fuels," *Journal of Propulsion and Power*, vol. 29, no. 3, pp. 582–592, May-June 2013. [Online]. Available: https://dio.org/10.2514/1.B34924

[31] S. Whitmore and A. Bulcher, "Vacuum test of a novel green-propellant thruster for small spacecraft," *53rd AIAA/SAE/ASEE Joint Propulsion Conference*, 2017.

[32] S. Whitmore, "Three-dimensional printing of "green" fuels for low-cost small spacecraft propulsion systems," *Journal of Spacecraft and Rockets*, vol. 54, 2017. [Online]. Available: https://doi.org/10.2514/1.A33782

[33] T. G. Beckwith, R. D. Marangoni, and J. H. Lienhard V, *Mechnical Measurements*, 6th ed.   Prentice Hall, 2006, pp. 85–145.

APPENDICES

APPENDIX A

Peng-Robinson Model

This appendix will detail the method used in Karabeyoglu [4]. This method, called the Peng-Robinson Model, stems from an equation of state, EOS, developed by Ding-Yu Peng and Donald B. Robinson [22].

A.1 Formulation of the Equation Of State

For semi-empirical equations of state the pressure is typically expressed as the sum of the repulsion pressure P_R and the attraction pressure P_A

$$P = P_R + P_A \tag{A.1}$$

From the van der Waals equation, developed in 1873, the repulsion pressure can be defined by the van der Waals hard sphere equation

$$P_R = \frac{RT}{\nu - b} \tag{A.2}$$

Thus the attraction pressure can be defined as

$$P_A = -\frac{a}{g(\nu)} \tag{A.3}$$

Here $g(\nu)$ is a function of the molar volume ν, b is a constant related to the size of the hard spheres, and a is the inter-molecular attraction force. Expressions for a and b can be obtained when applying Eq. A.1 at the critical point where the first and second derivatives of pressure with respect to volume disappear. Normally b is temperature independent, and therefore constant, and a is only treated as a constant in the van der Waals equation, thus it must be a function of temperature T. Therefore, Peng and Robinson propose Eq. A.4 as the equation of state.

$$P = \frac{RT}{\nu - b} - \frac{a(T)}{\nu(\nu + b) + b(\nu - b)} \tag{A.4}$$

A.2 Karabeyoglu Method

In Eq. A.4 R represents the gas constant. This EOS was used by Karabeyoglu because of the simplicity and higher accuracy at high pressures for determining properties of equilibrium mixtures of Nytrox compared to other EOSs that exist. For convenience, Eq. A.4 can be represented in cubic form

$$Z^3 - (1 - B)Z^2 + (A - 3B^2 - 2B)Z - (AB - B^2 - B^3) = 0 \tag{A.5}$$

The coefficients of A and B are expressed as

$$A = \frac{aP}{R^2T^2}, \quad B = \frac{bP}{RT} \tag{A.6}$$

And Z, the compressibility, is defined as

$$Z = \frac{P\nu}{RT} \tag{A.7}$$

With this problem dealing in the two phase region, the smallest positive root of Eq. A.5 relates to the compressibility of the liquid phase, and the largest root relates to that of the liquid.

When the critical point is reached, a, b, and Z become

$$a(T_c) = 0.45724 \frac{R^2T_c^2}{P_c}, \quad b(T_c) = 0.0778 \frac{RT_c}{P_c}, \quad Z_c = 0.307 \tag{A.8}$$

At all other temperatures the coefficients a and b are defined as

$$a(T) = a(T_c)\alpha(T_r, \omega), \quad b(T) = b(T_c) \tag{A.9}$$

Here α is dimensionless and a function of the reduced temperature T_r, represented as $T_r = \frac{T}{T_c}$, and ω which is the acentric factor for the particular molecule being used. At the critical point α is equal to unity.

The fugacity f of a pure component can be found by applying the thermodynamic relationship shown in Eq. A.10 to Eq. A.4 to yield Eq. A.11.

$$\ln \frac{f}{P} = \int_0^P \left(\frac{\nu}{RT} - \frac{1}{P} \right) dP \tag{A.10}$$

$$\ln \left(\frac{f}{P} \right) = Z - 1 - \ln(Z - B) - \frac{A}{2\sqrt{2}B} \ln \left(\frac{Z + 2.414B}{Z - 0.414B} \right) \tag{A.11}$$

To determine a functional form of $\alpha(T_r, \omega)$, the Newton's method was employed to solve the equilibrium condition of $f^L = f^v$ with a convergence criterion of $|f^L - f^v| \geq 10^{-4} kPa$. After convergence was met, a relationship between α and T_r was noted and linearized to be

$$\alpha^{1/2} = 1 + m(1 - T_r^{1/2}) \tag{A.12}$$

Here m is a constant for each substance used and is represented by

$$m = 0.37464 + 1.54226\omega - 0.26992\omega^2 \tag{A.13}$$

A.3 Mixing Rule

A single parameter mixing rule, k_{12}, needs to be used with the Peng-Robinson EOS to result in predictions that very closely match experimental data. The mixing rule used by Karabeyoglu was developed by Zudkevitch and Joffe [23]. This mixing rule is commonly used for the prediction of properties dealing with non-ideal solutions of fluids.

$$a = \sum_{i=1}^{N} \sum_{j=1}^{N} x_i x_j a_{ij} \tag{A.14}$$

$$b = \sum_{i=1}^{N} x_i b_i \tag{A.15}$$

$$a_{ij} = (1 - k_{ij})(a_i a_j)^{1/2} \tag{A.16}$$

From this mixing rule x_{ij} represents the mole fraction of the ith component, and k_{ij} is the interaction coefficient between molecules. In an ideal solution, k_{ij} is zero and any deviation from zero represents a strong molecular interaction. With this mixing rule in place an updated equation for the fugacity of the kth component can be determined

$$\ln\left(\frac{k_k}{Px_k}\right) = \frac{b_k}{b}(Z-1) - \ln(Z-B) - \frac{A}{2\sqrt{2}B}\left(\frac{2\sum_{i=1}^{N} x_i a_{ik}}{a} - \frac{b_k}{b}\right)\ln\left(\frac{Z + 2.414B}{Z - 0.414B}\right) \tag{A.17}$$

A.4   Nytrox Application

The following parameters can be used for nitrous oxide and oxygen mixtures

$$\omega_{N_2O} = 0.162, \quad (T_c)_{N_2O} = 309.6K, \quad (P_c)_{N_2O} = 71.6atm$$

$$\omega_{O_2} = 0.02, \quad (T_c)_{O_2} = 154.7K, \quad (P_c)_{O_2} = 49.8atm$$

After applying those parameters to the mixing rule previously defined in Section A.3, the mixing rule equations can be reduced and used to solve the properties of Nytrox mixtures

$$a = a_{O_2}x_{O_2}^2 + 2a_{12}x_{O_2}(1 - x_{O_2}) + a_{N_2O}(1 - x_{O_2})^2 \tag{A.18}$$

$$b = b_{O_2}x_{O_2} + bN_2O(1 - x_{O_2}) \tag{A.19}$$

$$a_{12} = (1 - k_{12})(a_{O_2}a_{N_2O})^{1/2} \tag{A.20}$$